https://doi.org/10.1016/j.engstruct.2022.115142

Hybrid welded T-section stub columns with Q690 flange and Q355 web: Testing, modelling and design

Jun-zhi Liu[a,d]; Shuxian Chen[b]; Tak-Ming Chan[b,c] *

[a] School of National Safety and Emergency Management, Bejing Normal University, China

[b] Department of Civil and Environmental Engineering, The Hong Kong Polytechnic University, Hong Kong, China

[c] Chinese National Engineering Research Centre for Steel Construction (Hong Kong Branch), The Hong Kong Polytechnic University, Hong Kong, China

[d] Department of Civil and Environmental Engineering, The Hong Kong Polytechnic University, Hong Kong, China

* Corresponding author: tak-ming.chan@polyu.edu.hk

Abstract

Comprehensive experimental and numerical investigations on hybrid T-section stub columns under compressive load were performed and are presented in this paper. The hybrid welded T-section stub columns comprise high strength steel Q690 flange and normal strength steel Q355 web. Material property studies were implemented through tensile coupon tests. Residual stress in membrane type was measured and recorded and its impact on structural performance was also assessed. Initial local geometric imperfection measurements were conducted for all the specimens. In conjunction with experimental studies, numerical investigation was performed to generate more test specimens extending the range of cross-section dimensions by which test data pool can be supplemented. The Eurocode of EN 1993-1-1, EN 1993-1-5 and EN 1993-1-12, the North American code of ANSI/AISC 360-16 and the Australian code of AS 4100 together with design approaches of Direct Strength Method and Continuous Strength Method were examined for its applicability for cross-section classification and compression resistance predictions of hybrid T-sections. Overall, the current specified limits were applicable for hybrid welded T-section and strength predictions from design codes were comparatively consistent and reliable. Strength predictions from Direct Strength Method and Continuous Strength Method were relatively appropriate though overly conservative predictions were provided for cross-section with large slenderness. In this study, modifications on the Direct Strength Method and Continuous Strength Method are proposed, which is shown to provide accurate predictions at cross-sectional level in a reliable manner.

1. Introduction

Increasing use of high strength steel (HSS) is witnessed by numerous applications of structural engineering and architectural design. Numerous advantages are presented by HSS structures such as high strength-to-weight ratio, reduced dimensions, reduced cost of erection/transportation, and decreased consumption of non-renewable resources [1,2]. The characteristics of the HSS make them a preferred option by the architect and engineers, particularly for the application in large-span and high-rise structures [3]. Despite the advantages possessed by HSS, relatively high price and less ductile mechanical behaviour limit its application. Hybrid section is one of the preeminent alternatives as it bring about a plenty of advantages including the economy efficiency and improved structural performance [4,5]. The experimental investigations on local buckling capacity of HSS hybrid section with the flange produced from SM570Q (nominal yield strength = 460 MPa) and web made from lower yield strength plate SM 400 (nominal yield strength = 235 MPa) was performed by Ito et al. [6]. It is of worthy noting that the hybrid sections exhibit better deformation capacity than the homogeneous counterparts made up from high-strength steel plates with same strength grade only. Hybrid girders did not show sudden decrease in terms of moment-inelastic rotation relationship after reaching the peak load. The local buckling behaviour of hybrid I-section was investigated with strength grade of web varied between 355 MPa and 690 MPa by Bartsch et al. [7]. It was found that hybrid sections generally exhibit better deformation capacity than the homogeneous counterpart comprising higher strength steel with regard to the normalised strength moment ratio and rotation capacity. For instance, the specimens of 203 and 204 were featured with normalised moment ratio of 1.19

and 1.16 with corresponding normalised rotation ratio of 6.18 and 5.97 respectively whereas their counterpart specimens of 103 and 104 provide normalised moment ratio of 1.15 and 1.13 with rotation ratios of 5.28 and 3.94 which are significantly lower than the hybrid sections.

Moreover, welded hybrid steel columns with the flange produced from A514 and A441, and webs made from A36 and A441 have been investigated by Nagarajarao et al. [8], the A514, A441 and A36 are featured with nominal yield strength of 460, 345 and 250 MPa respectively. It is however noted that the introduced investigations were focusing on doubly-symmetric hybrid sections, investigations into singly-symmetric hybrid sections is fairly limited. T-sections are commonly used in roof truss structures and lattice members of offshore and onshore structures [9, 10]. An example of the application of the T-section structural members in composite bridge is shown in Fig. 1. The relatively simple section facilitates its flexibility in modern construction. Local buckling performance of normal strength steel (NSS) T-section columns have been studied in Chen [11] and interactive buckling of NSS T-section columns was also investigated [12]. Post buckling strength and effective section method for NSS T-section column was examined by Trahair [13]. To study the member behaviour, experimental investigation into HSS columns in T-shaped sections with nominal yield strength of 800 MPa was conducted by Cao et al. [14]. Local stability of the HSS stub columns in T-section has been investigated by Liu et al. [15]. Hybrid T-section stub columns with the flange made of high strength steel Q690 and web made of Q460 were studied at cross-sectional level by Liu et al. [16], it was found that design specifications in EN 1993-1-12, ANSI/AISC 360-16 and AS 4100 can be extended to the cross-section classification for hybrid high strength steel T-section. Besides, HSS aluminum T-section columns under axial load was investigated by Yuan and Zhang [17]. Hybrid T-sections with the flange made from high strength plate can resist higher induced stress and the less onerous stress can be addressed by NSS plate in the web, resulting in combined advantage of greater ductility and structural efficiency than the homogeneous counterpart under flexure loads as beam-column members. Despite the potential advantages of hybrid T-sections in structural application, limited research has been carried out and no experimental investigations concerning local bucking of hybrid T-section comprising HSS Q690 flange and NSS Q355 web has been performed. Though, conclusions have been made in previous studies that current design specifications can be extended to the cross-section classification for hybrid high strength steel T-section with both flange and web made from high strength steel (greater than 460 MPa), it is unknown whether the design rules and cross-section classification slenderness limit can be extended to hybrid T-section comprising NSS web and HSS flange. Moreover, it should be noted that the specified contents for high-strength steel in design specifications EN 1993-1-12 [18] simply extended the design framework from NSS in EN 1993-1-1 [19]. Though design specifications are provided in EN 1993-1-5 [20] for hybrid girders, no design information is provided for hybrid T-sections which limit its engineering applications. The main purpose of this paper is to better understand the local buckling behaviour and the cross-section resistance for welded hybrid T-sections under pure axial compression. The fundamental information such as the effect of geometric imperfection and residual stress as well as structural performance at cross-sectional stage paves the path of extension to other loading conditions such as pure bending with constant moment, moment gradient, combined axial compression and bending in future research. The applicability of the design specifications for doubly symmetric sections were re-assessed and evaluated for the welded hybrid T-section.

2. Experimental investigation

2.1. Hybrid specimens made from Q690 and Q355

To study the local stability and compression resistance, 15 hybrid T-section stub columns were prepared and tested under concentric compression load. There are many fabrication routes to form the T-sections, such as directly welding two separate plates, cutting from the hot-rolled sections, or connecting two angle sections back-to-back through welding or mechanical fasteners. In this study, the examined T-sections specimens were cut from the hybrid I-sections using a wire-cutting machine with minimal heat input induced. The hybrid welded I-section were fabricated by welding the HSS

plates of Q690 and the NSS plates of Q355 through gas metal arc welding (GMAW). The parent plates were cut using plasma and the thicknesses of the parent plates were 10 mm and 6 mm for Q690 and Q355 respectively. The selected electrode is in the category of ER70S-6 with nominal yield strength of 470 MPa and ultimate strength of 580 MPa. The detailed chemical compositions of the parent plates of Q690 and Q355 and the selected electrode are shown in Tables 1 – 2 and Table 3 respectively. It should be noted that the electrode matching in hybrid sections should be complied with the web strength (lower strength grade), which is also commonly used in practice [5]. A labelling system was adopted in this study to identify the specimen with dimensions of the cross-section used in this paper. The letter "T" is used to represent the hybrid T-section stub columns, "690" and "355" after the hyphen indicates the strength grade of the flange and the web comprising the hybrid specimens. Following the strength grade after the hyphen, nominal dimensions of the height and the nominal thickness of the web are presented in a form of ($H \times t_w$, in mm). For example, a label of "T-690-355-150 × 6" indicates a hybrid T-section specimen consisting of Q690 flange and Q355 web with outer section height of 150 mm, and the nominal thickness of the web is 6 mm as shown in Fig. 2. The symbol "#" represents the identical stub column specimen for repeated testing. The actual dimensions of the studied hybrid sections using nomenclature in Fig. 2 were measured as shown in Table 4.

2.2. Material testing

The material properties of the parent plates were obtained through carrying out tensile coupon tests. Tensile coupon specimens were machined from the parent plates longitudinally and transversely by a water jet cutting machine, by which thermal effect and heat treatment can be excluded. The longitudinal tensile coupons were labelled as "TC-L-1, TC-L-2 and TC-L-3" whereas the transverse tensile coupons were labelled as "TC-T-1, TC-T-2 and TC-T-3". The letter "TC" indicates the tensile coupons, and the letters of "L" and "T " indicate the longitudinal and transverse direction. The number following after the hyphen implies the sequence number of the coupon taken from the parent plates. The dimensions of the tensile coupons were determined according to the specifications of EN 6892-1:2019 [21]. The widths of 13 mm and 8 mm along the parallel gauge length respectively was designed for specimens extracted from 6 mm and 10 mm thick plates for parent coupons, as presented in Fig. 3.

To conduct the tensile coupon test, Instron 5982, a universal testing system with a capacity of 100 kN was employed. Experimental arrangement of the tensile coupon test is shown in Fig. 4. The displacement-controlled load was applied with constant loading rate of 0.05 mm/min at initial stage and a relatively faster speed of 0.08 mm/min was used after the nominal yield strength [22, 23]. Elastic modulus and the strain development history can be derived based on the strain records. The obtained stress-strain curves for Q355 and Q690 steel materials are shown in Fig. 5 respectively. The experimentally tested material properties of the parent plates are reported in Table 5 and Table 6.

2.3. Geometric imperfections

Initial local geometric imperfection, which formed during manufacturing, transportation and handling, was measured for each welded hybrid T-section stub column. Experimental arrangement of the initial local imperfection measurement is shown in Fig. 6, similar arrangement has been successfully applied in [24, 25]. The specimen was mounted on a milling machine platform and a set of three Linear Variable Displacement Transducers (LVDTs) using a specially developed fixtures moved along the length of the specimen. Two LVDTs were located near the edges of the web or flange and one LVDT is located at the axial centreline of the plate. To avoid possible local imperfection near ends of specimen, the measurement was started from a certain distance at about 20 mm from both edges. The amplitude of imperfection was determined based on the deviation from the measured points and the average values from the edge side measurements and the maximum amplitudes (ω_0) of the local geometric imperfection are reported in last column of Table 4.

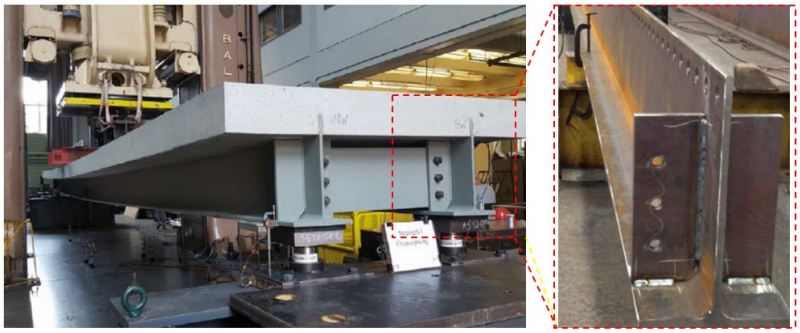

Fig. 1. An example of composite bridge deck comprising steel T-section components [9].

Table 1 Chemical compositions listed in mill certificate for 10 mm thick Q690 parent plates.

Steel plate	Chemical composition										
	C (%)	Mn (%)	P (%)	S (%)	Si (%)	Cr (%)	Mo (%)	Nb (%)	Ti (%)	B (%)	CEV
10 mm plate	0.14	1.40	0.019	0.001	0.27	0.26	0.15	0.024	0.013	0.002	0.46

Table 2 Chemical compositions listed in mill certificate for 6 mm thick Q355 parent plates.

Steel plate	Chemical composition								
	C (%)	Mn (%)	P (%)	S (%)	Si (%)	Cr (%)	Ni (%)	Cu (%)	CEV
6 mm plate	0.17	1.34	0.019	0.010	0.24	0.21	0.011	0.064	0.44

Table 3 Chemical compositions of the welding electrode ER70S-6 for hybrid sections.

Electrode	Chemical composition				
	C (%)	Si (%)	Mn (%)	P (%)	S (%)
ER70S-6	0.08	1.00	1.50	0.012	0.010

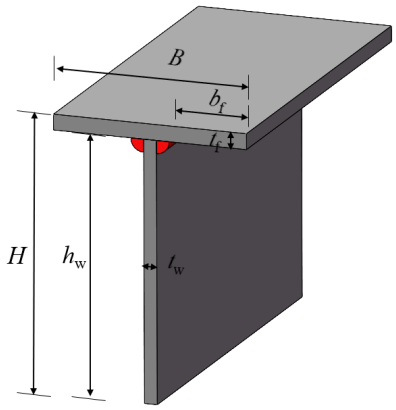

Fig. 2. Notations of the hybrid welded T-section.

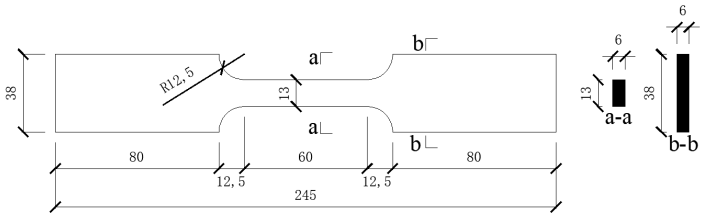

(a)

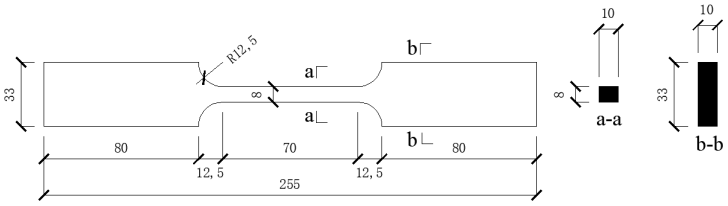

(b)

Fig. 3. Dimensions of flat coupon specimens taken from the parent steel plates, in mm (a) Flat coupon specimen taken from the 6 mm steel plate (b) Flat coupon specimen taken from the 10 mm steel plate.

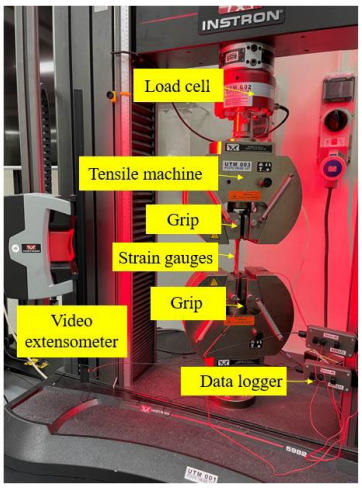

Fig. 4. Test arrangement of the tensile coupon specimen.

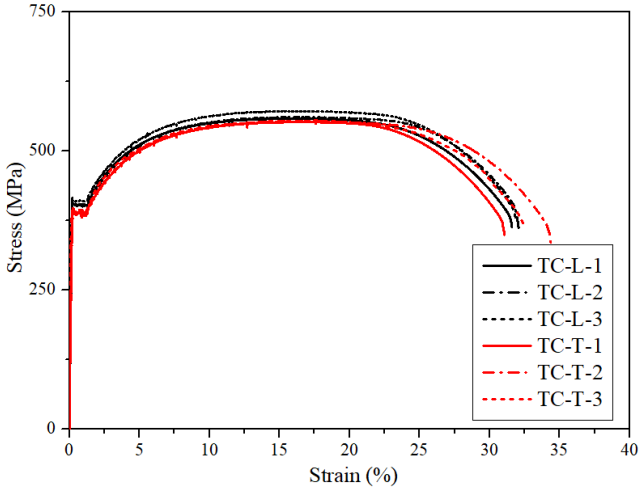

(a)

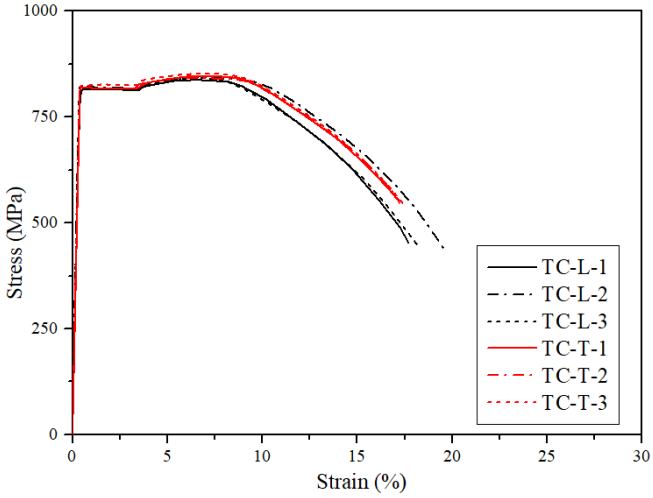

(b)

Fig. 5. Measured stress-strain curves of (a) tensile coupons of 6 mm thick parent plate (b) tensile coupons of 10 mm parent plate.

Table 4 Measured geometric dimensions of hybrid T-section stub column specimens.

Specimens	L (mm)	B (mm)	H (mm)	b_f (mm)	h_w (mm)	t_f (mm)	t_w (mm)	ω_0 (mm)
T-690-355-45 × 6	200.1	109.8	44.9	42.4	26.1	9.66	6.72	0.23
T-690-355-50 × 6	200.2	109.7	50.1	43.5	32.4	9.68	6.71	0.19
T-690-355-55 × 6	200.1	109.8	54.9	43.1	36.8	9.67	6.70	0.22
T-690-355-60 × 6	200.2	109.8	60.1	43.8	42.7	9.66	6.71	0.28
T-690-355-65 × 6	299.9	109.9	64.9	44.1	47.7	9.67	6.71	0.27
T-690-355-70 × 6	300.1	109.9	69.8	44.4	52.9	9.68	6.70	0.18
T-690-355-70 × 6#	300.2	109.9	69.9	44.5	53.1	9.68	6.70	0.22
T-690-355-75 × 6	300.2	109.9	75.1	43.2	57.0	9.66	6.71	0.26
T-690-355-80 × 6	300.1	109.8	80.3	42.8	61.9	9.65	6.72	0.28
T-690-355-80 × 6#	300.2	109.9	80.2	42.8	61.8	9.65	6.72	0.26
T-690-355-100 × 6	300.2	109.8	100.3	44.8	83.9	9.66	6.72	0.33
T-690-355-120 × 6	400.1	109.8	120.1	44.8	103.7	9.67	6.71	0.42
T-690-355-150 × 6	399.9	109.9	149.8	43.8	132.3	9.66	6.71	0.38
T-690-355-170 × 6	449.9	109.9	170.1	43.3	152.1	9.67	6.72	0.41
T-690-355-200 × 6	545.5	109.7	200.3	43.2	182.3	9.66	6.72	0.45

Note: # indicates the repeated test

Table 5 Mean measured material properties from 6 mm thick Q355 parent plates.

Section	E_s (GPa)	f_y (MPa)	f_u (MPa)	ε_u (%)	ε_f (%)	ε_{sh} (%)
Longitudinal	220.1	403	564	15.6	31.6	1.36
Transverse	213.2	382	553	17.2	32.0	1.24

Table 6 Mean measured material properties from 6 mm thick Q690 parent plates.

Section	E_s (GPa)	f_y (MPa)	f_u (MPa)	ε_u (%)	ε_f (%)	ε_{sh} (%)
Longitudinal	216.1	815	843	6.7	18.4	3.52
Transverse	217.4	819	848	6.7	18.3	3.42

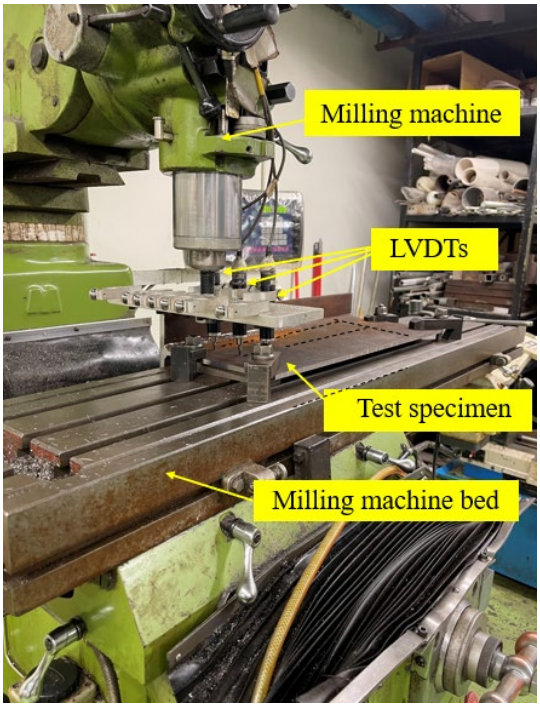

Fig. 6. Setup of local geometric imperfection measurements for HSS hybrid welded T-section.

2.4 Membrane residual stress

Membrane residual stress can be caused by the welding process due to the restraint of unheated area to the heated zone and elongation along the welding direction. The effect of the fabrication route (e.g., wire cutting the T-section from the welded I-section) on the structural behaviour of the hybrid T-section stub columns in this study was also examined by residual stresses investigation. Membrane residual stress may lead to premature failure of the structural members, the characteristic distributions and its magnitudes were therefore measured and recorded. Sectioning method using wire-cutting was conducted to measure the membrane residual stress for hybrid T-sections of T-690-355-115 × 6 and T-690-355-155 × 6 in accordance with the recommendations specified in Ziemian [26]. The strips were marked in the longitudinal direction concerning the stress gradient. The strain gauges were affixed to the mid-height on both sides of strips with waterproof tape covered and the coolant was applied to remove the heat. The readings of strain gauges were recorded prior to the cutting process. The strains were then recorded again when the locked internal strains were released after cutting. Five times measurements were conducted with the maximum and minimum values deducted and the average values of the remaining recorded data were used. The strains before and after cutting were recorded and the differences were considered to be the released inter-locked elastic strain. The magnitudes of membrane residual stresses were determined by multiplying the measured Young's modulus, given in Eq. (1).

$$\sigma_{\mathrm{m}} = - \left(\frac{\Delta\varepsilon_{\mathrm{ext}} + \Delta\varepsilon_{\mathrm{int}}}{2}\right) E_{\mathrm{s}} \quad (1)$$

where $\Delta\varepsilon_{\mathrm{ext}}$ is the derivatives after removing the initial strain readings from the final srain readings for external strain gauge, $\Delta\varepsilon_{\mathrm{int}}$ is the same derivatives but for internal strain gauge. The experimentally measured amplitudes and distribution of the membrane residual stress for two sections of T-690-355-115 × 6 and T-690-355-155 × 6 are presented in Fig. 7.

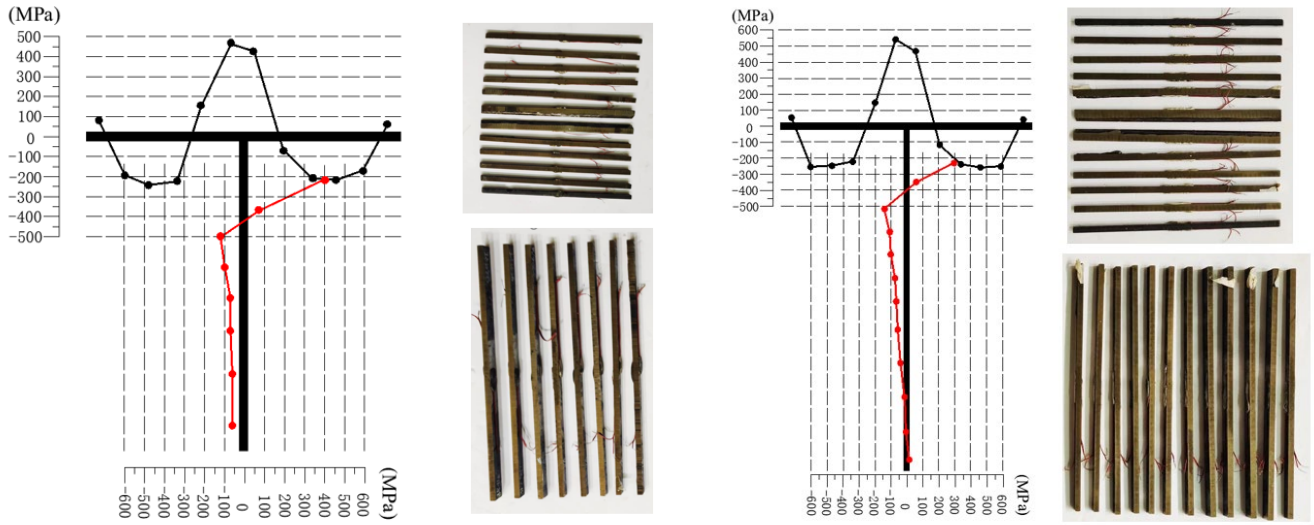

(a) T-690-355-115 × 6 (b) T-690-355-155 × 6

Fig. 7. Test results of the residual stress patterns and amplitudes.

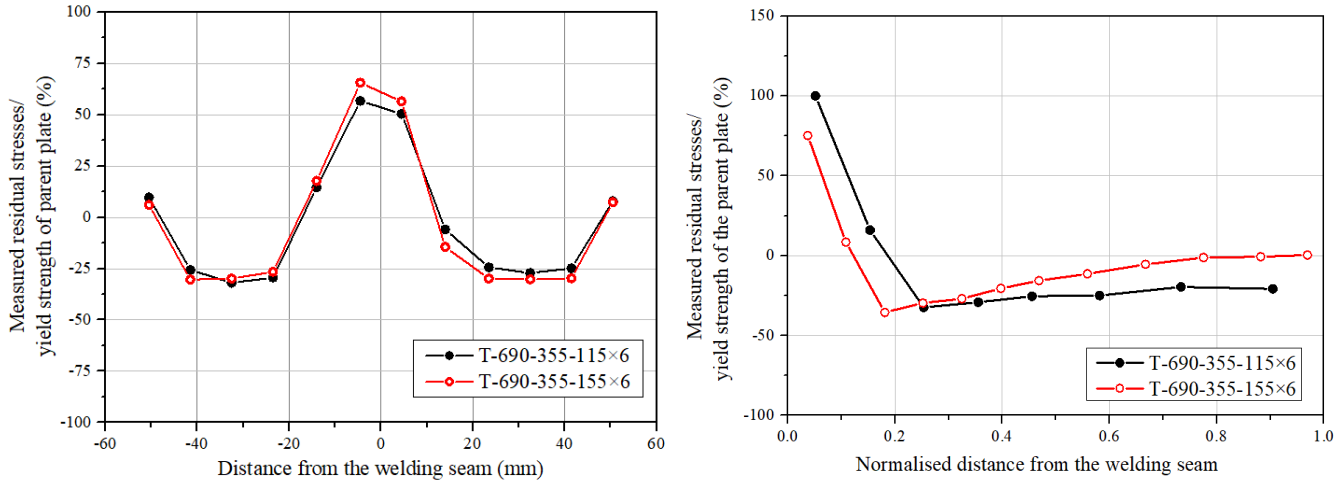

(a) (b)

Fig. 8. Normalised residual stress distributions along the distance from the welding seam in (a) flange (b)web.

The measured residual stresses were plotted in a normalisation form (normalised to yield strength of the parent plates and distance from welding seam) as shown in Fig. 8. The highest magnitude of membrane residual strain has outreached the yield strain, attaining 100% of the yield strength (entering the yield plateau) of web plate in the strip next to the welding region whereas the membrane residual stress near welding for flange are relatively lower approximately equal to 63% of its yield strength. It should be noted that the residual stress near the weld metal will reach yielding level for normal strength steels [27]. Two specimens display similar distribution pattern that the largest tensile membrane residual stresses, as anticipated, were observed near the welding region and the magnitudes show a gradually decreased tendency both for flange and web away from the welding seam and then change to compressive stress. Based on the obtained results, a membrane residual stress predictive model for hybrid T-section is proposed to facilitate its application (in sub-section of 3.2).

2.5. Stub column tests

A total of 15 stub column tests were carried out to investigate the local buckling behaviour and cross-section resistance. To ensure the applied compressive load could be uniformly distributed to the stub columns, the end sections of the stub

columns were milled flat prior to the testing. Furthermore, the end fixtures were employed to clamp the end section of the examined specimens as a precaution against premature buckling at the end. The detailed configuration of the end fixture is illustrated in Fig. 9(a). The HSS bolts were used to tighten the end of the specimens. The nominal length of the stub column is determined as three times the largest dimension of the cross-section which is deemed to be sufficient long to contain representative geometric imperfections and residual stresses during fabrication but suitably short enough to avoid global buckling [28, 32]. To apply the compressive load, an MTS rock mechanics testing system with a capacity of 5000 kN was used. Test arrangements comprised four LVDTs with 50 mm range and seven strain gauges adhering to the mid-height of the specimen by which the end shortening of the stub column specimens can be measured by LVDTs and the longitudinal strain under axial compressive load can be obtained by strain gauges. Three strain gauges were affixed to the flange with one in the middle and the other two were located near the edge of outstand flat elements. The other four strain gauges were arranged on each side of the web plate, with one near the middle of the flat portion and the other one near the edge of the bottom of the web, as shown in Fig. 9(a) in the axonometric and sectional view. The test set-up of the investigated stub column specimens is shown in Fig. 9(b). The axial load was realised through displacement-controlled with a constant loading rate of 0.2mm/min adopted for all the specimens [33]. The pre-loading test was conducted prior to the formal compressive loading with the loading rate of 0.1mm/min until the 10% of the approximate yield load, aiming to check whether experimental instrumentations are correct and work well. The strain gauges were also used to detect the initiation of local buckling, determination of the local buckling load as well as aligning the stub column specimen to ensure that the compressive load passes through its centroid point. The relationship of the axial load and longitudinal strain for the typical hybrid T-section stub column specimen is plotted in Fig. 10. Based on the graph, it was observed that the compressive strains for all the seven strain gauges consistently increase under the axial compressive load at early elastic stage until the occurrence of local buckling. The compressive strain corresponding to the location where local buckling occurred start to display an inverse tendency and the dashed cross indicates the determined local buckling load as shown in Fig. 10. The local buckling load for all the hybrid T-section stub columns were determined and the results are reported in Table 7, denoted as N_{lb}. Based on the obtained results, the hybrid T-section columns with slender web were characterised with lower local buckling load prior to the attainment of the yield load. It is of worthy mentioning that the local buckling failure of the web does not lead to the overall failure of the cross-section. Under the same loading condition of compressive stress gradient, the web plate with lower strength grade enters the plasticity stage first while the flange comprising high strength steel remain in elastic stage. The web plate may experience the either elastic local buckling due to the slender cross sections or local buckling after reaching the yield load. For hybrid T-section stub columns of T-690-355-70 × 6, T-690-355-80 × 6, T-690-355-100 × 6 and T-690-355-120 × 6, the normalised ratio of N_{lb} to $N_{u,test}$ is lower than the unity, indicating the local buckling occur before the attaining of the yield load. Nevertheless, the ultimate cross-sectional resistances still outreach the yield load of the cross-sections, principally attributed to the element interaction effect from the flange plate, of which the failed web plate was supported and restrained from the adjacent plate members.

Moreover, true end shortenings of the stub column specimens were derived by removing the inherently contained elastic deformation of the end bearing plates from LVDTs based on the strain gauge readings [29]. The relationship between axial load and end shortening curves of the tested specimens are plotted in Fig. 11. Table 7 reports the key test results including the ultimate axial load $N_{u,test}$, the end shortening at ultimate load δ_u, yield load N_y and the ultimate to yield load ratio $N_{u,test}/N_y$. In determination of the yield load N_y, an equivalent yield strength f_y^* was used which is weighted by strength and the area of the respective plates of different strength grades. The equivalent yield strength f_y^* equals to $(A_{,f} \times f_{y,f} + A_{,w} \times f_{y,w})/(A_{,f} + A_{,w})$, where $f_{y,f}$ is the 0.2% proof strength of the flange and $f_{y,w}$ is the 0.2% proof strength of the web, $A_{,f}$ and $A_{,w}$ are the area of flange and web respectively. The normalised ratio of ultimate to yield load $N_{u,test}/N_y$ implies the failure modes of the stub columns. If the normalised ratios are higher than the unity, the investigated specimens are considered failed by local buckling upon reaching the yield load. Alternatively, the specimens are regarded failed by elastic local buckling prior to the attainment of the yield load. As observed in Fig. 12, local buckling mode of T-section under compression is characterised by the buckled web plate in the middle and flange was buckled towards

inside and outside alternatively.

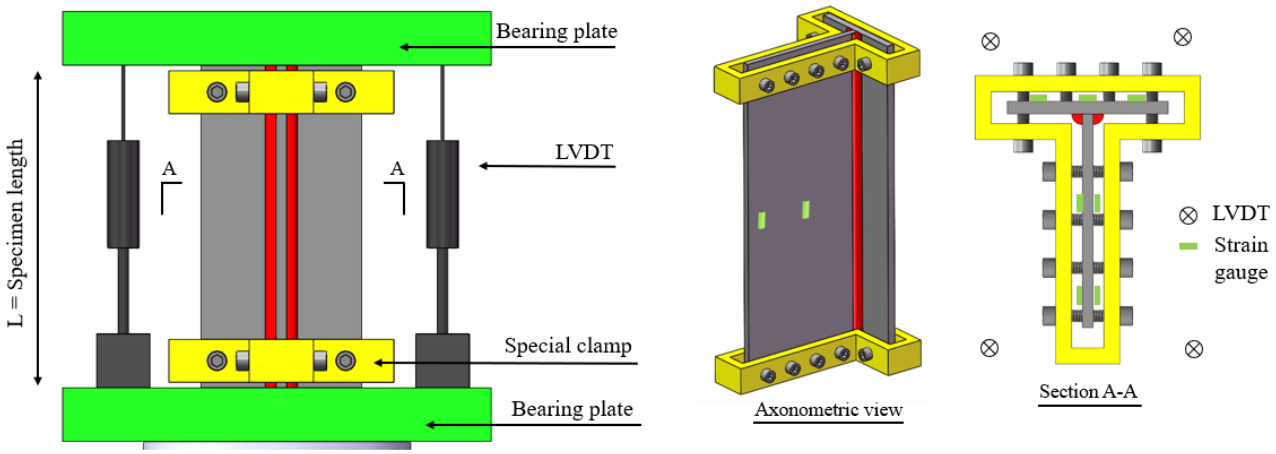

(a) Schematic arrangement

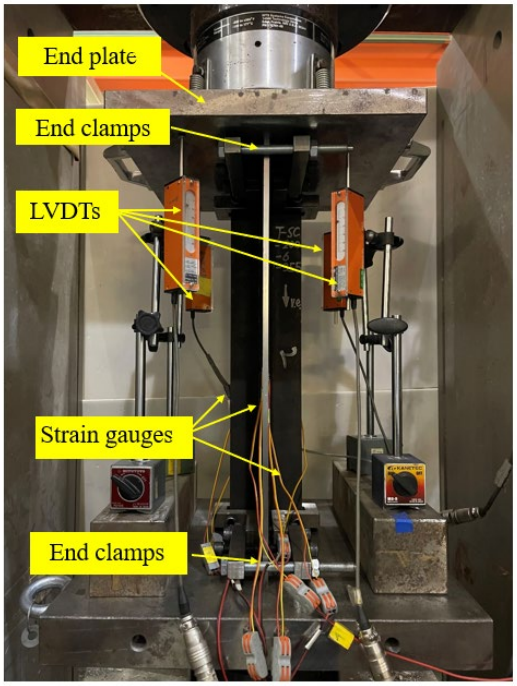

(b) Experimental arrangement

Fig. 9. Test set-up for hybrid welded T-section stub column.

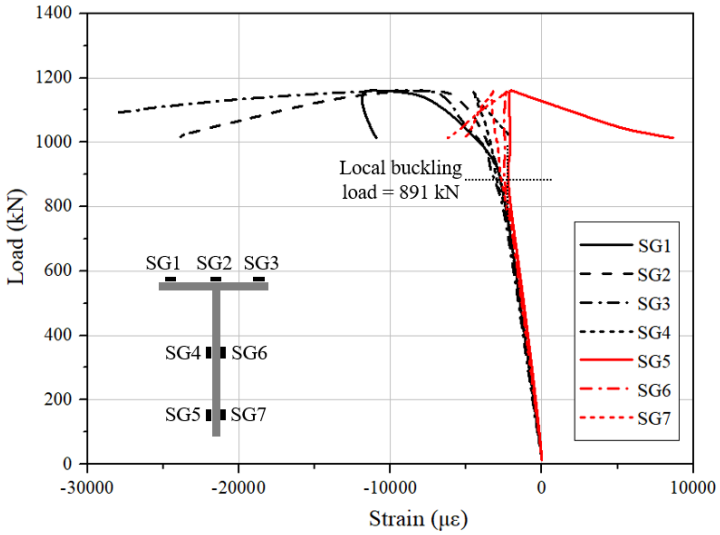

Fig. 10. Load-strain curves of hybrid HSS welded T-section stub column specimen of T-690-355-100 × 6.

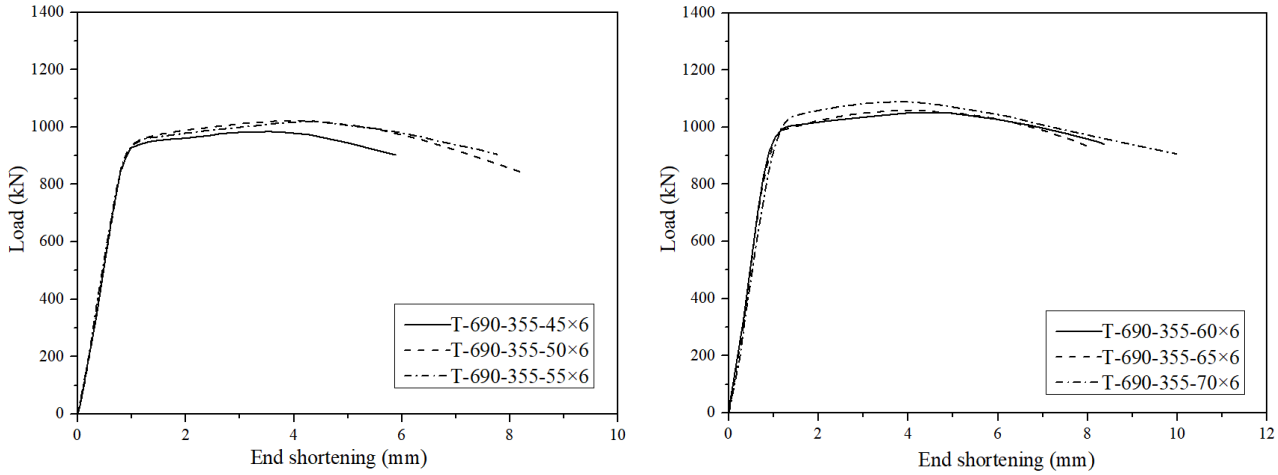

(a) Specimen with height of 45 mm, 50 mm and 55 mm (b) Specimen with height of 60 mm, 65 mm and 70 mm

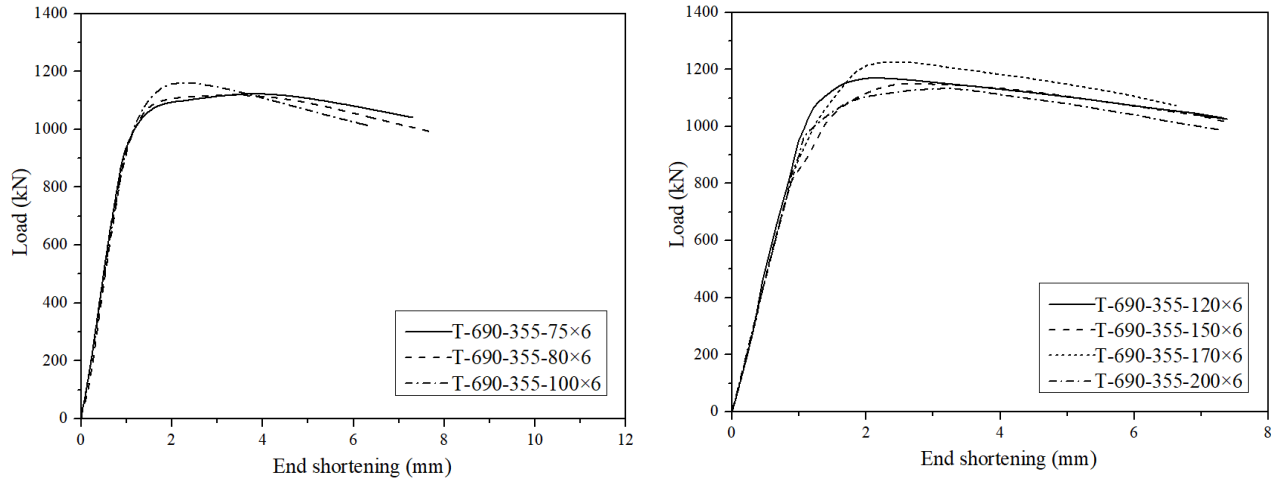

(c) Specimen with height of 75 mm, 80 mm and 100 mm (d) Specimen with height of 120 mm, 150 mm, 170 mm and 200mm

Fig. 11. Relationship between the axial load and end shortening of the investigated stub columns.

Fig. 12. Typical local buckling mode of representative specimens.

Table 7 Summary of the test results of the investigated stub columns.

Specimens	$N_{u,test}$ (kN)	δ_u (mm)	$N_{u,test}/Af_y^*$	N_{lb} (kN)	$N_{lb}/N_{u,test}$
T-690-355-45 × 6	991.2	3.39	1.03	N.A.	N.A.
T-690-355-50 × 6	1063.1	3.91	1.09	N.A.	N.A.
T-690-355-55 × 6	1025.9	3.95	1.04	N.A.	N.A.
T-690-355-60 × 6	1056.8	3.87	1.05	N.A.	N.A.
T-690-355-65 × 6	1066.1	4.20	1.09	1050.5	0.985
T-690-355-70 × 6	1088.9	3.86	1.06	1008.5	0.926
T-690-355-70 × 6#	1090.0	3.84	1.06	1010.2	0.927
T-690-355-75 × 6	1123.1	3.82	1.08	930.2	0.828
T-690-355-80 × 6	1118.7	3.30	1.06	868.8	0.777
T-690-355-80 × 6#	1119.1	3.25	1.06	866.5	0.774
T-690-355-100 × 6	1160.7	2.30	1.05	891.5	0.768
T-690-355-120 × 6	1173.2	2.44	1.01	1002.1	0.854
T-690-355-150 × 6	1150.5	2.66	0.93	782.5	0.680
T-690-355-170 × 6	1206.8	2.52	0.93	755.8	0.626
T-690-355-200 × 6	1132.8	3.74	0.82	610.5	0.539

Note: Note: # indicates the repeated test; f_y^* is the equivalent yield strength which equals to $(A_{,f} \times f_{y,f} + A_{,w} \times f_{y,w})/(A_{,f} + A_{,w})$, where $f_{y,f}$ is the 0.2% proof strength of the flange and $f_{y,w}$ is the 0.2% proof strength of the web; N.A. indicates that local buckling load are not applicable for these stocky sections.

3. Numerical studies

3.1. General

In conjunction with the physical compressive tests, extensive numerical simulation investigations were carried out using

finite element (FE) analysis through a commercially available software ABAQUS. The validation studies encompass (i) Developing the FE models; (ii) Validating the FE model using the test results; (iii) Conducting the parametric studies with a larger spectrum of dimensions.

3.2. Numerical modelling

The measured geometric properties were modelled to replicate each stub column specimen. Mean material properties were determined based on the obtained results from parent plates and then used in FE models. The tested engineering stress-strain relationships were converted to true stress and plastic strain which was subsequently input in FE for material modeling. The reduced integration shell element S4R, a four-noded curved thin or thick shell elements with reduced integration suitable for complex buckling analysis, was used in FE models for all the specimens. The S4R shell element has six degrees of freedom per node and was extensively used in previous investigations with accurate predictions [30, 31, 40, 41]. To strike a good balance between the computational cost and numerical accuracy, sensitivity study pertaining the mesh size was conducted with element size selected from $h_w/30$, $h_w/25$, $h_w/20$, $h_w/15$ and $h_w/10$. An element size equalling to $h_w/20$ was consequently employed in FE analysis as it can reduce computational time but maintain numerical accuracy. Comply with the boundary condition set-up for hybrid stub columns in the experiment, the end sections of specimens were fixed against all translation and rotations except for the axial direction at one end to allow for displacement -controlled load, as shown in Fig. 13. Special attention was paid to the location of the reference point, which was in line with the centroid of the cross section and was carefully determined with the areas of the web and flange. Linear elastic buckling eigan value analysis was performed to obtain the lowest elastic buckling eigen mode under compression which was then taken as the representative distributed profile of initial local geometric imperfection, as shown in Fig. 14. The measured initial local geometric imperfections were subsequently incorporated into the FE model by multiplying the first eigen mode. After completion of the linear bucking analysis, non-linear buckling analysis (GMNIA) were conducted using RIKS step specifying the axial displacement. The geometries of the fillet welds were considered in the FE models using the method of additional shell elements with varying thickness [15]. To account for the effect of the membrane residual stress, it was introduced into the FE model as initial state using either command of 'initial condition' or 'keywords' file. Fig. 15 shows a typical distribution pattern and magnitudes after incorporating the membrane residual stress in FE model of T-690−355-120 × 6. The predictive model of the residual stress distribution of hybrid T-section is proposed and the net force is zero. The membrane residual tensile stress at the middle of the top flange and the top of the web is the same to maintain compatibility. The impact of the membrane residual stresses on the structural behaviour of the T-sections was executed by comparing the results from FE model with or without inclusion of membrane residual stresses for all the tested specimens. Fig. 16 shows the comparison of load-end shortening responses of the representative specimen of T-690−355-120 × 6. It was found that FE models with inclusion of residual stress led to 2% decrease in ultimate strength with earlier yielding of the cross section on average, but the path of the deformation curves were almost identical. The comparison of the load ratio of $N_{u,FE}/N_{u,test}$ for all the tested specimens are summarised in Table. 8 based on measured initial local imperfections. It was observed that intermediate and slender sections were more sensitive to the initial local imperfections. This phenomenon could be principally due to the earlier local buckling of the web plate occurred prior to the attainment of the yield load. The membrane residual stresses lead to premature local buckling by superposition of the inter-locking residual stress with the external applied compressive load for slender sections whereas widespread plasticity after yielding induces stress redistribution, partially counteracting the impact of the residual stress. Furthermore, the web plate of hybrid T-section comprised mild steel which was characterised with distinct strain hardening. The plasticity of the web plate section has been fully developed when the whole cross-section enters the stage of the yield load (reaching the yield load $A f_y^*$). Overall, the mean value of the normalised load ratio $N_{u,FE}/N_{u,test}$ with or without inclusion of membrane residual stresses are 0.98 and 0.99 with corresponding coefficient of variations of 0.016 and 0.021. It can then be concluded that the effect of membrane residual stress is negligible. Therefore, it is unnecessary to explicitly include the membrane residual stress in the further parametric studies for simplicity. Similar conclusions have also been concluded in previous study for welded I-section

in Sun et al. [3].

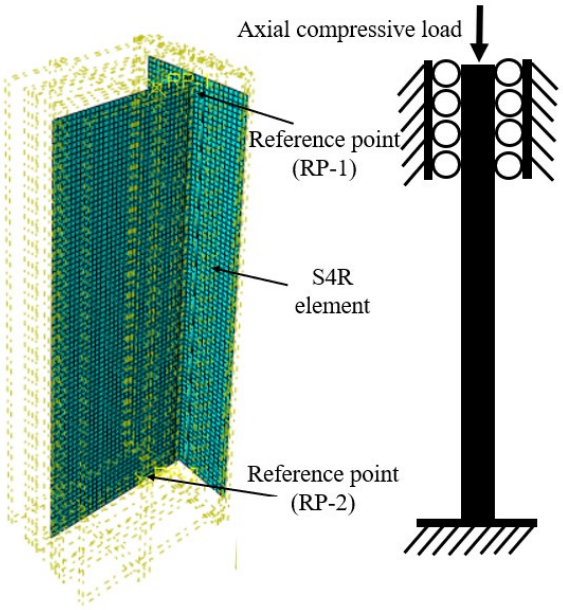

Fig. 13. Illustrations of the mesh and boundary conditions in FE analysis.

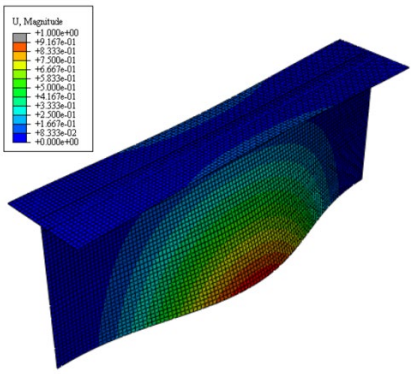

Fig. 14. Typical first buckling mode shape generated from Eigenvalue analysis (U in mm).

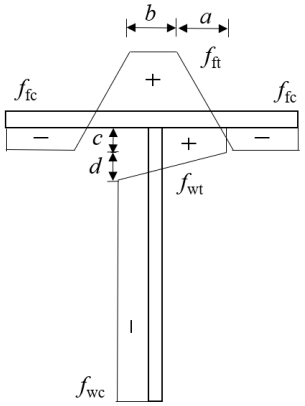

$f_{ft} = 0.5f_{y,f}$
$f_{wt} = 1.0f_{y,w}$
f_{fc} = From equilibrium
f_{wc} = From equilibrium
$a = 0.205B$
$b = 0.185B$
$c = 0.095h_w$
$d = 0.195h_w$

(a) predictive model

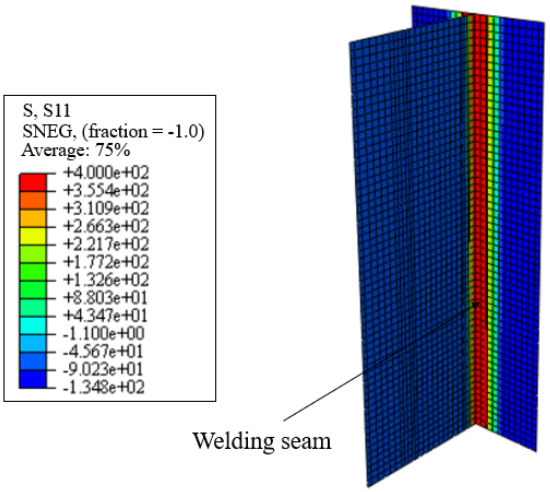

(b) Typical distribution incorporated in T-690−355-120 × 6

Fig. 15. Membrane residual stress modeling in FE.

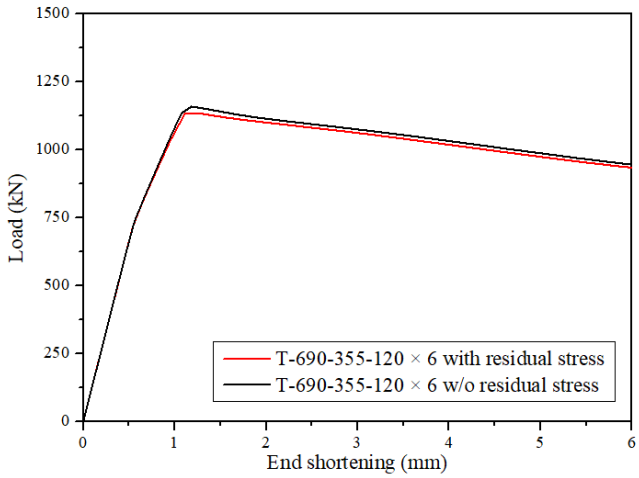

Fig. 16. Comparison of the load-end shortening response for T-HSC-120 × 6 with or without residual stress.

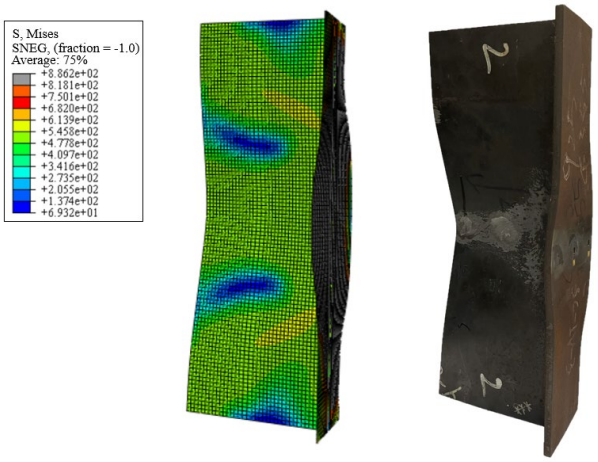

Fig. 17. Comparison of the failure mode for the section T-690-355-200 × 6.

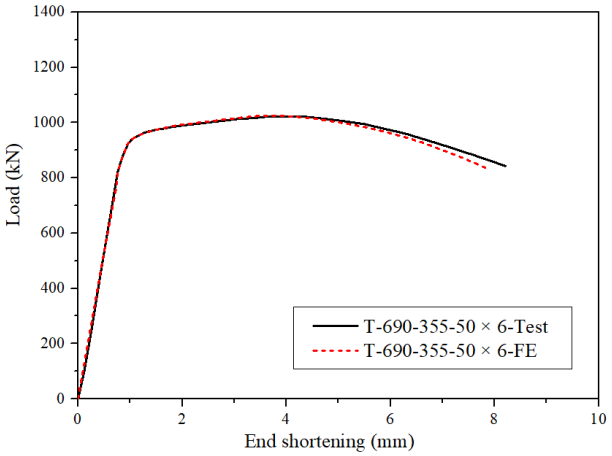

(a) Specimen of T-690-355-50 × 6

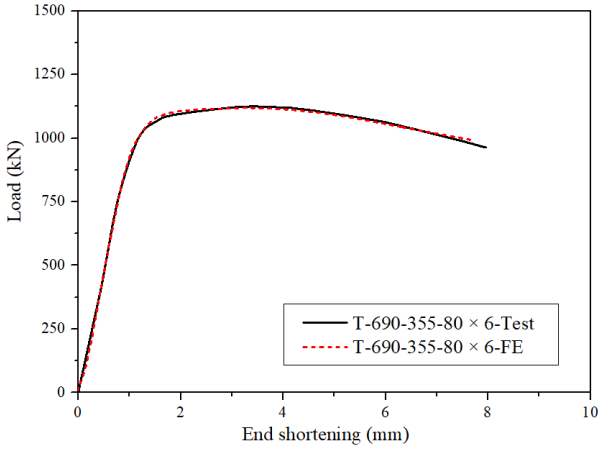

(b) Specimen of T-690-355-80 × 6

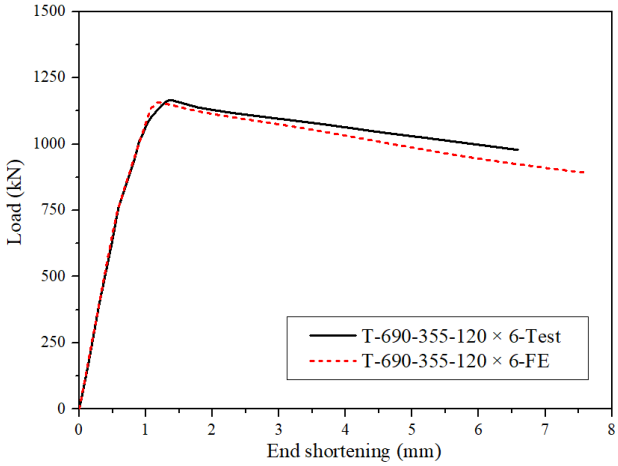

(c) Specimen of T-690-355-120 × 6

Fig. 18. Comparison of the experimental and numerical load-end shortening responses.

3.3. Validation analysis

Comparison of experimental and FE failure mode for the section T-690-355-200 × 6 is presented in Fig. 17 that excellent agreement can be observed. Fig. 18 presents the comparison between the experimental and numerical axial load-end shortening responses of hybrid welded T-section stub columns of T-690-355-50 × 6, T-690-355-80 × 6 and T-690-355-120 × 6 respectively. It was found that ultimate loads from the experiments can be accurately predicted from the FE models and the load-end shortening curves correlate well with each other. Furthermore, imperfection sensitivity analysis was also performed to determine the optimal imperfection magnitude to be incorporated into FE analysis. Four imperfection values including measured local geometric imperfection value ω_0, and three imperfection values expressed by the fraction of the plate thickness $t_w/10$, $t_w/50$, as well as $t_w/100$ were assessed and compared. FE-to-test load ratios for the tested specimens are summarised in Table 8. Mean values of $N_{u,FE}/N_{u,test}$ of the tested specimens among four considered initial local imperfection magnitudes are 0.99, 0.98, 0.99 and 1.00 respectively with corresponding CoVs of 0.021, 0.024, 0.022 and 0.020 respectively. Though the four studied imperfection values yield precise and consistent predictions, imperfection value of $t_w/10$ was employed as it provides reliable predictions compared with the other three imperfection magnitudes on conservative side.

3.4. Parametric studies

The validated FE models developed in sub-section of 3.3 were used to perform parametric studies, with primary aim at supplementing the database by generating structural performance data covering a broader range of cross-sectional dimensions. The elastic critical buckling stress for flange in T-section is $\sigma_{cr,f} = k_f \frac{\pi^2 E}{12(1-v^2)(b_f / t_f)^2}$ and $\sigma_{cr,w} = k_w \frac{\pi^2 E}{12(1-v^2)(h_w / t_w)^2}$ for web plate respectively subject to compression. Therefore, when $b_f/h_w = (k_w/k_f)^{0.5}$ the elastic critical buckling stress of flange and web is the same. For the case in this study, the buckling coefficient of k_f and k_w are the same, equal to 0.43 for outstand flat element under pure compression. Hence, no interaction will occur as the b_f and h_w are the same. The cross-sectional resistance will benefit from the interaction effect from the shorter plate element with the restraint from the flange when the h_w is larger than the b_f. The modelled hybrid T-section specimens were thereafter featured with a fixed flange width equal to 110 mm for consistent comparison. In particular, the yield strength of the flange and web plate should be accounted for in assessing the cross-section classification. To determine the slenderness of the flange $b_f/t\varepsilon$ and web plates $h_w/t\varepsilon$, where $\varepsilon = (235/f_y)^{0.5}$ and the measured yield strength of Q690 and Q355 were used respectively. The variations of the section slenderness were achieved by changing the length of the web from 51 mm to 212 mm, resulting in a broader web slenderness range between 6.28 and 37.5 and the aspect ratio varied from 0.46 to 1.93. The slenderness ratios of the flange plate to web plates are also reported in the Table 9. It should be noted that for specimens with outer height larger than 64 mm, the web plate governs the overall cross-section classification with slenderness ratio of 8.8 while the slenderness of the flange is a constant value of 8.2. For the cross-section with height less than 64 mm (51 mm to 60 mm in Table 9), the flange governs the cross-section classification and design. The detailed information concerning the parametric studies were reported in Table 9, resulting in 83 FE models in total. The generated FE results and the experimental test data were used together to evaluate the applicability and suitability of the current structural steel design codes and the developed advanced design approaches of DSM and CSM.

Table 8 Sensitivity analysis of the initial local imperfection amplitudes and residual stresses.

Specimens	$N_{u,FE}/N_{u,test}$					
	ω_0	$t_w/10$	$t_w/50$	$t_w/100$	Membrane residual stress	No membrane residual stress
T-690-355-45 × 6	0.98	0.98	0.98	0.99	0.98	0.98
T-690-355-50 × 6	0.99	0.98	0.99	0.99	0.99	0.99
T-690-355-55 × 6	1.00	0.99	1.00	1.00	0.99	1.00
T-690-355-60 × 6	0.99	0.98	0.99	0.99	0.98	0.99
T-690-355-65 × 6	0.99	0.98	0.99	0.99	0.98	0.99
T-690-355-70 × 6	0.99	0.97	0.99	0.99	0.98	0.99
T-690-355-70 × 6#	0.99	0.97	0.99	0.99	0.98	0.99
T-690-355-75 × 6	0.97	0.95	0.96	0.97	0.96	0.97
T-690-355-80 × 6	0.99	0.98	0.99	0.99	0.97	0.99
T-690-355-80 × 6#	0.99	0.98	0.99	0.99	0.97	0.99
T-690-355-100 × 6	0.99	0.99	1.00	1.00	0.97	0.99
T-690-355-120 × 6	0.97	0.97	0.98	0.99	0.95	0.97
T-690-355-150 × 6	1.03	1.03	1.04	1.04	1.00	1.03
T-690-355-170 × 6	0.97	0.97	0.98	0.98	0.94	0.97
T-690-355-200 × 6	1.05	1.05	1.05	1.05	0.99	1.05
Mean	0.99	0.98	0.99	1.00	0.98	0.99

CoV			0.021	0.024	0.022	0.020	0.016	0.021

Note: # indicates the repeated test

Table 9 Cross-section geometric dimensions selected for parametric study.

Cross-section dimensions			Element slenderness		Slenderness ratio	Aspect ratio	Height
B	t_w	t_f	$h_w/t\varepsilon$	$b_f/t\varepsilon$	$\frac{h_w/t\varepsilon}{b_f/t\varepsilon}$	α	H (mm)
(mm)	(mm)	(mm)					
110	6	10	6.28-37.5	8.03	0.74, 0.76, 0.79, 0.81, 0.83, 0.86, 0.88, 0.90, 0.93, 0.95, 0.98, 1.07, 1.12, 1.16, 1.21, 1.26, 1.31, 1.35, 1.40, 1.45, 1.49, 1.54, 1.59, 1.64, 1.68, 1.73, 1.78, 1.82, 1.87, 1.92, 1.97, 2.01, 2.06, 2.11, 2.16, 2.20, 2.25, 2.30, 2.34, 2.39, 2.44, 2.49, 2.53, 2.58, 2.63, 2.67, 2.72, 2.77, 2.82, 2.87, 2.92, 2.97, 3.02, 3.07, 3.12, 3.17, 3.22, 3.27, 3.32, 3.37, 3.42, 3.47, 3.52, 3.57, 3.62, 3.67, 3.72, 3.77, 3.82, 3.87, 3.92, 3.97, 4.02, 4.07, 4.12, 4.17, 4.22, 4.27, 4.32, 4.37, 4.42, 4.47, 4.52	0.46-1.93	51, 52, 53, 54, 55, 56, 57, 58, 59, 60, 64, 66, 68, 70, 72, 74, 76, 78, 80, 82, 84, 86, 88, 90, 92, 94, 96, 98, 100, 102, 104, 106, 108, 110, 112, 114, 116, 118, 120, 122, 124, 126, 128, 130, 132, 134, 136, 138, 140, 142, 144, 146, 148, 150, 152, 154, 156, 158, 160, 162, 164, 166, 168, 170, 172, 174, 176, 178, 180, 182, 184, 186, 188, 190, 192, 194, 196, 198, 200, 202, 204, 206, 208, 210, 212

4. Evaluation of the current design codes and design approaches

4.1. General

The applicability and suitability of the existing design provisions in design codes of EN 1993-1-1 [19], EN 1993-1-5 [20], EN 1993-1-12 [18], ANSI/AISC 360-16 [34] as well as AS 4100 [35] against 15 experimental data and 83 FE results were assessed and compared. In addition to the design codes, design method of DSM, which can take account for the element interaction effect and CSM which is a deformation-based design method considering both strain hardening and interaction effect were also evaluated.

4.2 Cross-section classification

In the design framework of Eurocode EN 1993-1-1 [19], four cross-section classes were included in the classification framework. Class1, 2, and 3 sections are referred to the sections which can achieve the yield load whereas Class 4 sections are those sections which cannot attain the yield load due to local buckling. For Class 4 sections, partial section

of the structural element cannot resist the external load due to the occurrence of local buckling, the width b of the cross-section is thereby reduced to the effective width of b_{eff}. EN 1993-1-12 [18] simply extends the design specifications for normal strength steel to high strength steel design with strength grade up to S700. In the later section, design codes of EN 1993-1-1 and EN 1993-1-12 are referred as EC3. Different from Eurocode EC3, ANSI/AISC 360-16 [34] and AS 4100 [35] specify the cross-section under compression into two sections, namely non-slender and slender sections, allowing for structural steel design with nominal yield strength up to 690 MPa. Table 10 reports the codified cross-section yield slenderness limits for out-stand elements from various design codes. The experimental and numerical results were normalised to the corresponding squash load Af_y*, and subsequently plotted against the ratios of $b/(t\varepsilon_{\text{EC3}})$, $b/(t\varepsilon_{\text{AISC}})$ and $b/(t\varepsilon_{\text{AS4100}})$ in Fig. 19. In the classification framework of the design codes, the classification of the cross sections highly depends on its slenderest constituent plate element and then being used to compare with the width-to-thickness ratio b/t with codified slenderness limits, where b is the clear width of the plate element. Different material parameters such as $\varepsilon_{\text{EC3}} = (235/f_y)^{0.5}$, $\varepsilon_{\text{AISC}} = (E/f_y)^{0.5}$, and $\varepsilon_{\text{AS4100}} = (250/f_y)^{0.5}$ are used to account for the differences of the material strengths in various codes respectively. The average yield strength measured from the tensile coupon tests for flange and web were used respectively for each constituent plate members with different strength grades. Fig. 19 shows that the current codified slenderness limits in these design codes for slender/non-slender outstand flat elements are generally applicable for hybrid welded T-section under compression. Compared with ANSI/AISC 360-16, slenderness limits of EC3 and AS 4100 provide more reliable classification.

To deal with the plate elements subject to local buckling, effective width method is adopted in these design codes. Notwithstanding the concept of the effective width is considered in design codes to address the section susceptible to elastic local buckling, the equations to derive the effective width is different. EN 1993-1-1 [19] relates the effective width b_{eff} to the width b by using a cross-section slenderness parameter specified in EN 1993-1-5 [20], given in Eq. (2)

$$\bar{\lambda}_{\text{p}} = \frac{b/t}{28.4\varepsilon_{\text{EC3}}\sqrt{k_\sigma}} \tag{2}$$

where k_σ is the buckling factor which is equal to 0.43 for out-stand elements in this study. Then the effective width can be calculated following Eq. (3)

$$b_{\text{eff,EC3}} = b\left(\frac{1}{\bar{\lambda}_{\text{p}}} - \frac{0.188}{\bar{\lambda}_{\text{p}}^{\,2}}\right) \le b \tag{3}$$

The equations to determine the effective width in structural steel design codes of ANSI/AISC 360-16 [26] and AS 4100 [29] are given in Eq. (4) and Eq. (5),

$$b_{\text{eff,AISC}} = b\left(\frac{1.49\lambda_{\text{p,AISC}}}{\frac{b}{t}} - \frac{0.49\lambda_{\text{p,AISC}}^{\,2}}{\left(\frac{b}{t}\right)^2}\right) \le b \tag{4}$$

where $\lambda_{\text{p,AISC}}$ is the limiting width-to-thickness ratio specified in ANSI/AISC 360-16

$$b_{\text{eff,AS4100}} = b\left(\frac{14}{b/(t\varepsilon_{\text{AS4100}})}\right) \le b \tag{5}$$

Direct strength method (DSM) was originally developed for open section cold-formed structural members which need to find the governing buckling stress among various elastic bucking mode including elastic local buckling, global buckling, and distorsional buckling through numerical tools [36]. The obtained elastic buckling stress f_{cr} from the corresponding governing buckling mode are used to derive the non-dimensional cross-section slenderness $\lambda_{\text{p}} = (f_y/f_{\text{cr}})^{0.5}$. Using the determined cross-section slenderness, the cross-section resistance from DSM can be derived using Eq. (6). Different from DSM, continuous strength method (CSM) employs a base curve by which the cross-sectional slenderness parameter $\lambda_{\text{p}} = (f_y/f_{\text{cr}})^{0.5}$ can be related to the deformation capacity ($\varepsilon_{\text{csm}}/\varepsilon_y$) [37]. Experimental investigations including

columns and beam tests have been performed to construct the base curves corresponding to carbon- and stainless-steel materials [38, 39]. The hybrid sections comprise HSS flange and NSS web, it is therefore reasonable to adopt the base curve for flange and web respectively. The base curve applicable to HSS structural components was developed and proposed in Lan et al. [40] which was employed in this study for flange, as shown in Eq. (7). Concerning the NSS web, base curve corresponding for the hot-rolled steel should be used [41, 42] given in Eq. (8). The CSM limiting stress f_{csm} can be calculated from Eq. (9),

$$N_{DSM}=\begin{cases} f_y A & \text{for } \lambda_p \le 0.776 \\ 1-\dfrac{0.15}{\lambda_p^{0.8}})\dfrac{1}{\lambda_p^{0.8}} f_y A & \text{for } \lambda_p > 0.776 \end{cases} \tag{6}$$

$$\frac{\varepsilon_{csm}}{\varepsilon_y}=\begin{cases} \dfrac{0.294}{\lambda_p^{3.174}} \le \min(15, \dfrac{C_1\varepsilon_u}{\varepsilon_y}) & \text{for } \lambda_p \le 0.68 \\ (1-\dfrac{0.219}{\lambda_p^{1.014}})\dfrac{1}{\lambda_p^{1.014}} & \text{for } \lambda_p > 0.68 \end{cases} \tag{7}$$

$$\frac{\varepsilon_{csm}}{\varepsilon_y}=\begin{cases} \dfrac{0.25}{\lambda_p^{3.6}} \le \min(15, \dfrac{C_1\varepsilon_u}{\varepsilon_y}) & \text{for } \lambda_p \le 0.68 \\ (1-\dfrac{0.222}{\lambda_p^{1.05}})\dfrac{1}{\lambda_p^{1.05}} & \text{for } \lambda_p > 0.68 \end{cases} \tag{8}$$

$$f_{csm}=\begin{cases} E_s\varepsilon_{csm} & \text{for } \varepsilon_{csm} \le \varepsilon_y \\ f_y & \text{for } \varepsilon_y < \varepsilon_{csm} < \varepsilon_{sh} \\ f_y + E_{sh}(\varepsilon_{csm}-\varepsilon_{sh}) & \text{for } \varepsilon_{sh} < \varepsilon_{csm} < C_1\varepsilon_u \end{cases} \tag{9}$$

where E_s is Young's modulus, ε_y and ε_u are the strains at the yield and ultimate stresses, ε_{sh} is the strain hardening strain defined as the end of the yield plateau after which the strain hardening initiates, $C_1\varepsilon_u$ represents the strain at the intersection point. The other material coefficients C_2 is used to define the strain hardening modulus of E_{sh}, as given in Eq. (10).

$$E_{sh}=\frac{f_u-f_y}{C_2\varepsilon_u-\varepsilon_y} \tag{10}$$

CSM material model proposed in Chen et al. [1] for HSS was used for flange and material model for hot-rolled carbon steel of Q355 steel in Yun and Gardner [42] was applied to the web steel. The required parameters in determination of the material model for HSS and NSS materials are summarised in Table 11 and Table 12 respectively. Using the obtained CSM limiting stress, the stub column resistance predictions can be determined as given in Eq. (11).

$$N_{csm}=\begin{cases} f_{csm} A & \text{for } \lambda_p \le 0.68 \\ \dfrac{\varepsilon_{csm}}{\varepsilon_y} f_y A & \text{for } \lambda_p > 0.68 \end{cases} \tag{11}$$

Note that in the determination of the cross-section slenderness parameter λ_p, it comes to an issue that two different strength grades were essentially included in hybrid sections. Therefore, comparisons between the normalised cross-

section resistance and two different cross-section slenderness are compared in Figs. 19(b)-(c). It can be concluded that the specified limit value of DSM is non-conservative if λ_p is calculated based on the lower strength grade from the web whereas most data locate on the left side above the unity when λ_p is based on flange. The limit value of CSM based on web strength is more appropriate for classification of hybrid T-section stub columns that overly conservative predictions were obtained using flange strength.

Table 10 Slenderness limits between slender and non-slender plate elements in compression.

Design standards and methods	Yield slenderness limits
EN 1993-1-1 and EN 1993-1-12	$b/t \leqslant 14\varepsilon_{EC3}$
ANSI/AISC 360-16	$b/t \leqslant 0.64\varepsilon_{AISC}$
AS 4100	$b/t \leqslant 14\varepsilon_{AS4100}$
DSM	$\lambda_p = 0.776$
CSM	$\lambda_p = 0.68$

Table 11 CSM material model for HSS materials.

	ε_u	ε_{sh}	C_1	C_2
$0.85 < f_y/f_u \leqslant 0.9$	$0.8(1-\frac{f_y}{f_u})$	$0.2\frac{f_y}{f_u}+0.2$	$\frac{\varepsilon_{sh}+0.3(\varepsilon_u-\varepsilon_{sh})}{\varepsilon_u}$	$\frac{\varepsilon_{sh}+0.55(\varepsilon_u-\varepsilon_{sh})}{\varepsilon_u}$
$0.9 < f_y/f_u$	$1-\frac{f_y}{f_u}$	0.02		

Table 12 CSM material model for NSS material.

	ε_u	ε_{sh}	C_1	C_2
$f_y/f_u \leqslant 0.85$	$0.6(1-\frac{f_y}{f_u})$	$0.1\frac{f_y}{f_u}-0.055$	$\frac{\varepsilon_{sh}+0.25(\varepsilon_u-\varepsilon_{sh})}{\varepsilon_u}$	N.A.[a]

Note: a indicates that the material parameter of C_2 is not applicable for normal strength steel material

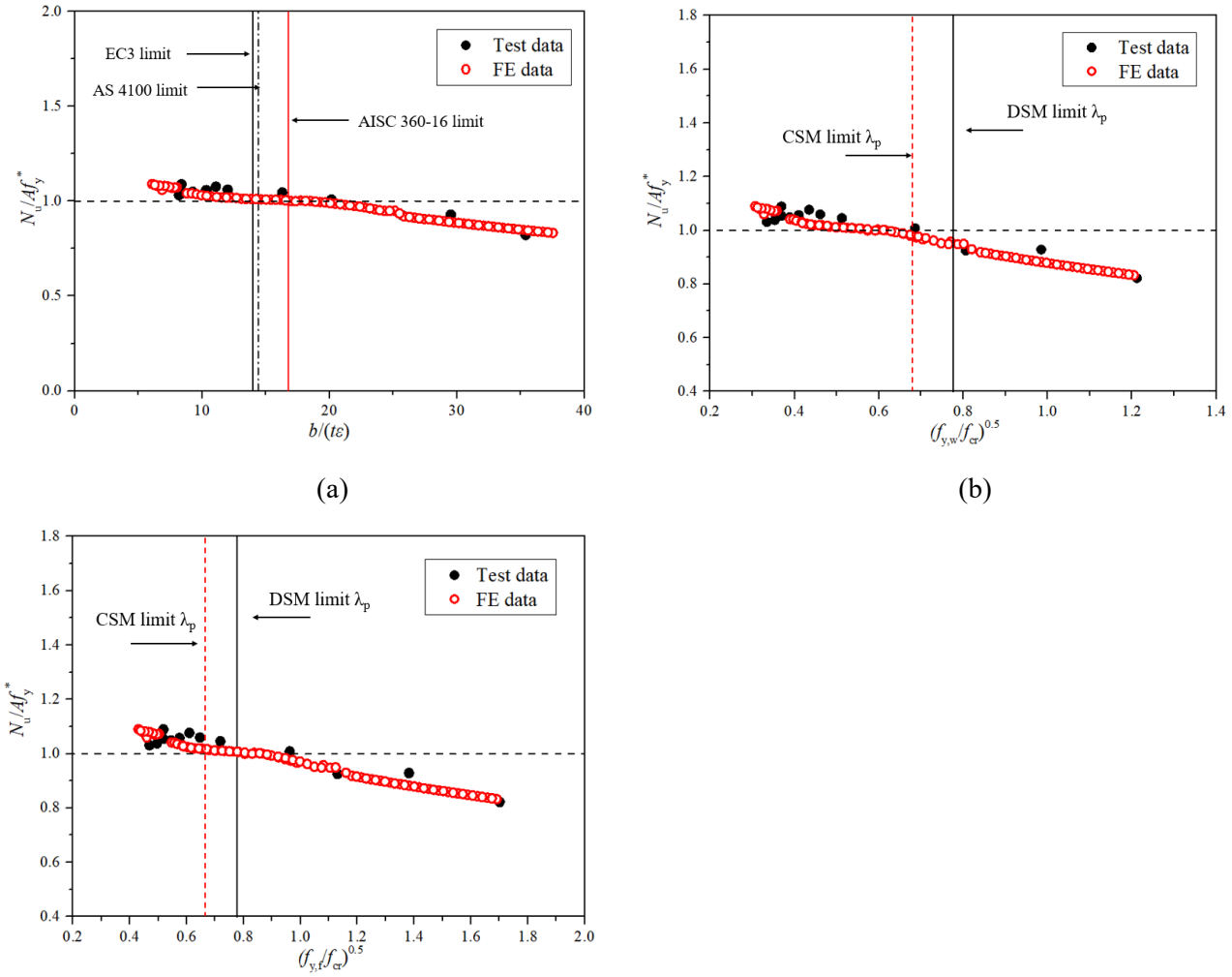

Fig. 19. Assessment of slenderness limit (a) Slenderness limits in design codes (b) DSM with slenderness obtained based. on strength from the web (c) DSM with slenderness obtained based on strength from the flange

4.3 Cross-section resistances

The relationship between the normalised load ratios and the corresponding plate slenderness are depicted in Figs. 20–22. Key results, including the mean (test and FE)-to-predicted ratios of $N_u/N_{u,pred}$, the corresponding coefficient of variations (CoVs) are shown in Table 13. The mean value of $N_u/N_{u,pred}$ obtained from design codes of EC3 and AS 4100 are 1.04 and 1.05 which is relatively higher than the 1.01 from AISC 360-16. Compared with EC3 and AISC 360-16, AS 4100 provide comparatively conservative predictions. All design codes yield rather accurate and consistent predictions which may be extended to cover compressive design of hybrid T-sections with Q690 flange and Q355 web. $N_{u,DSM}^*$ is the compressive resistance based on flange strength, and $N_{u,DSM}$ is determined based on the web strength. The mean values of $N_u/N_{,pred}$ obtained from DSM and DSM* are 1.02 and 1.16. The corresponding CoV from DSM is 0.040 which is lower than 0.113 from DSM*. The mean values of $N_u/N_{,pred}$ obtained from CSM and CSM* are 1.06 and 1.26 with CoVs of 0.069 and 0.160 respectively. For the sections with cross-section slenderness greater than 0.776, overly conservative results were derived based on current DSM design approach, as shown in Fig. 21. In comparison with DSM, CSM provide more accurate predictions for stocky sections as seen in Fig. 22 as anticipated taking account for strain hardening. Predictions for sections with λ_p larger than 0.68, the degree of conservatism is increasing as cross-section slenderness increases. Analogous to the DSM*, the CSM* based on flange strength provides overly conservative results for sections with λ_p larger than 0.68 and the predictions for sections with λ_p smaller than 0.68 are comparatively reliable, as shown in Fig. 22. The over-estimated cross-sectional resistance predictions from DSM and CSM indicate that the

modifications on design curves need to be further conducted for hybrid welded T-section stub columns under pure compression.

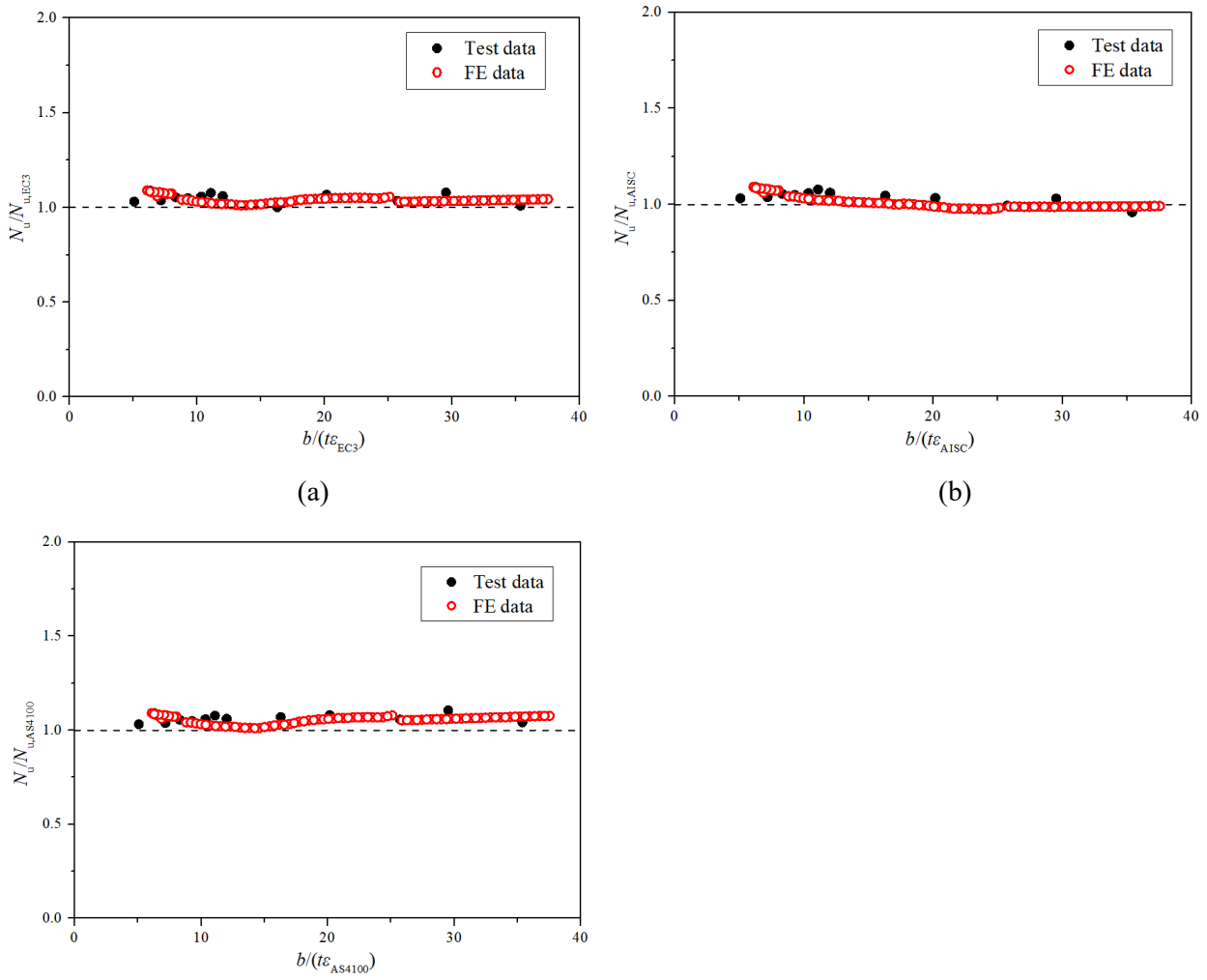

Fig. 20. Comparisons of experimental and numerical results with strength predictions from design codes (a) EC 3 (b) ANSI/AISC 360-16 (c) AS 4100.

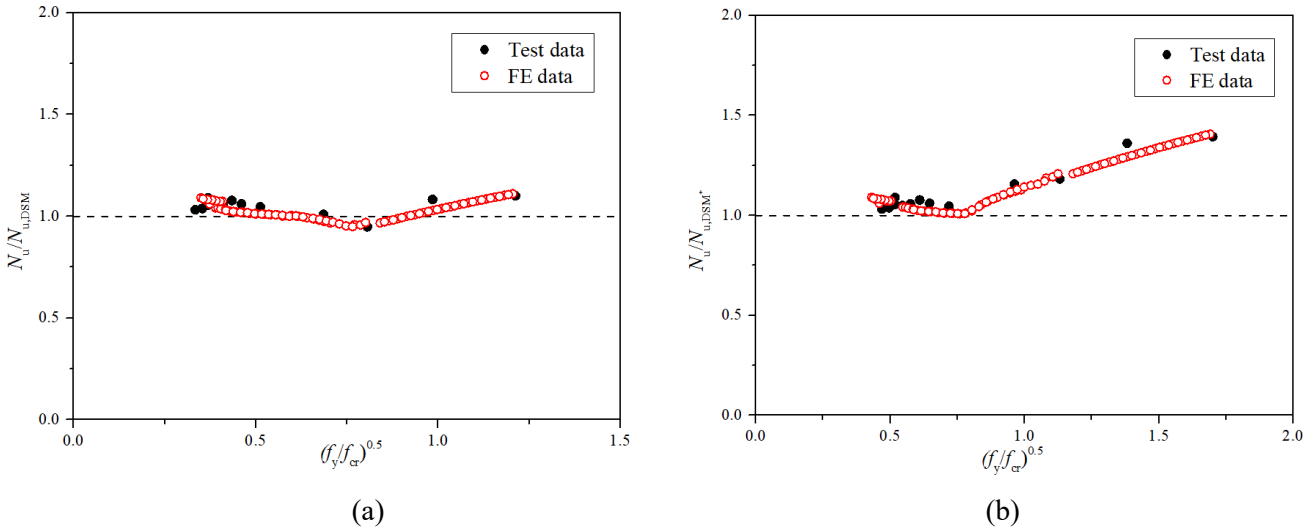

Fig. 21. Comparisons of strength predictions (a) DSM and (b)DSM*.

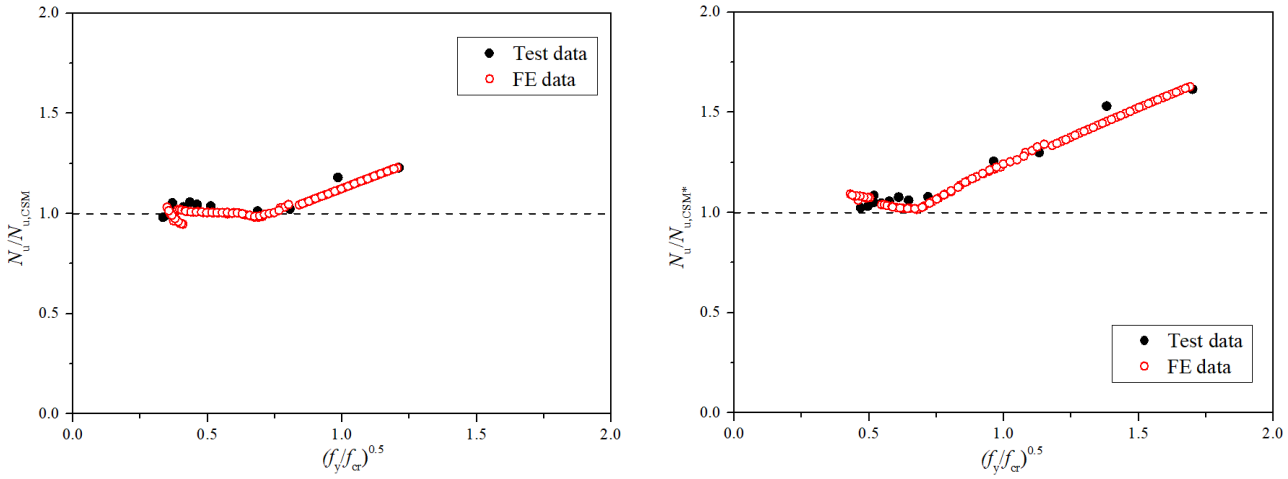

(a) (b)

Fig. 22. Comparisons of strength predictions (a) CSM and (b) CSM*.

4.4. Proposed modified design approaches of DSM and CSM

The present design approach of DSM provided either conservative or non-conservative predictions for non-slender and slender sections. The normalised load ratio of cross-sectional resistance under pure compression to the yield load ($N_y = Af_y^*$) are plotted against the slenderness of DSM with the original DSM design curve added in Fig. 23. It was observed that the current horizontal plateau of the limit value of unity cannot represent and capture the strain hardening behaviour of the non-slender hybrid T-section stub columns, particularly for sections with lower cross-section slenderness. A linear expression is proposed to replace the traditional limit value of the unity and compare with the test and FE data in Fig. 23 for non-slender sections. As can be seen in Fig. 23, the strain hardening and cross-sectional resistance of non-slender sections can be fully exploited by the newly proposed linear equation, as given in Eq. (12). Likewise, the obtained cross-sectional resistances of slender sections were normalised to the yield load and is plotted in Fig. 24 against the section slenderness. The original DSM curve overly predicted the cross-sectional resistance for hybrid T-section with cross-section slenderness ranging between 0.64 and 0.94 and subsequently provided conservative results for slender sections, with degree of conservatism increasing as cross-sectional slenderness increases. Hence, modified design equation is proposed for slender sections and compared against the test and FE data. Based on the comparison with the design predictions using the proposed modified DSM, notable improvement in cross-sectional resistance predictions can be seen in Fig. 25 and Table 13. The mean value of $N_u/N_{u,pred}$ obtained from modified DSM is 1.01 with corresponding CoV of 0.013. The reliability analysis was also conducted for the modified DSM and the required partial factor was equal to 1.0, indicating the proposed modified DSM is reliable.

$$N_{DSM,prop} = \begin{cases} (1.102 - 0.164\lambda_p) f_y A & \text{for } \lambda_p \le 0.64 \\ (1 - \frac{0.125}{\lambda_p^{0.336}}) \frac{1}{\lambda_p^{0.336}} f_y A & \text{for } \lambda_p > 0.64 \end{cases} \quad (12)$$

In addition to the proposed modified DSM, design approach of CSM was also modified for its applicability for the cross-sectional resistance design for hybrid T-section stub columns under concentric compression. The base curves for high strength and normal strength carbon steel were compared and assessed with structural performance data from non-slender hybrid T-sections, as shown in Fig. 26. It can be generally concluded that the existing base curve for NSS can accurately capture the deformation capacity of the investigated hybrid T-section. The CSM design curves for NSS and HSS were also compared and are plotted in Fig. 27. It was observed that the existing design curve provide over-conservative predictions. A new design curve is proposed based on regression analysis, as shown in Eq. (13). The applicability of the proposed modified CSM for hybrid T-section stub columns was assessed by comparing the

experimental and numerical results with the design predictions by the modified CSM, as shown in Fig. 28 and Table 13. The mean value of $N_u/N_{u,pred}$ obtained from modified DSM is 1.00 with corresponding CoV of 0.013. The reliability analysis was also conducted for the modified CSM with required partial factor equal to 1.0, indicating the proposed modified CSM is reliable. It should be noted that the slenderness used in proposed design approaches were determined based on the lower strength steel from the web plate, and the proposed slenderness limit value for DSM and CSM is 0.64.

$$\left(\frac{\varepsilon_{csm}}{\varepsilon_y}\right)_{prop} = \begin{cases} \dfrac{0.178}{\lambda_p^{3.877}} \le \min\left(15, \dfrac{C_1\varepsilon_u}{\varepsilon_y}\right) & \text{for } \lambda_p \le 0.64 \\ \left(1-\dfrac{0.125}{\lambda_p^{0.336}}\right)\dfrac{1}{\lambda_p^{0.336}} & \text{for } \lambda_p > 0.64 \end{cases} \tag{13}$$

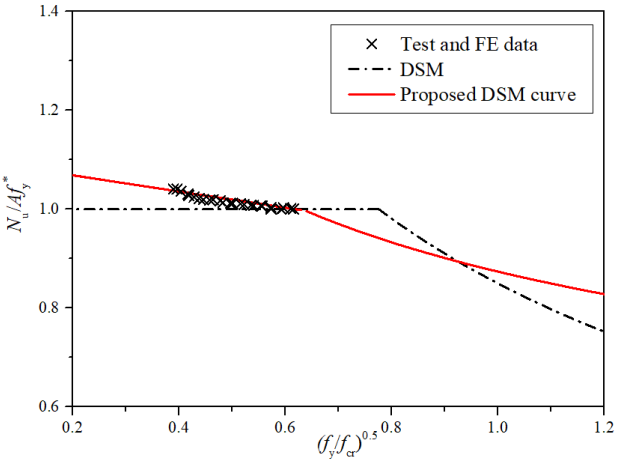

Fig. 23. Assessment of the proposed DSM for non-slender hybrid T-section under pure compression.

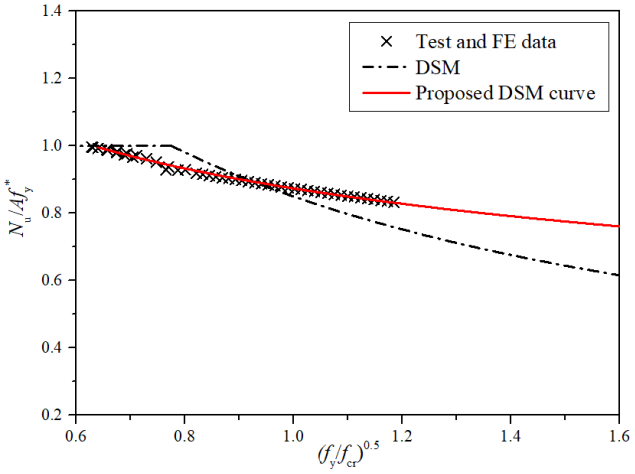

Fig. 24. Assessment of the proposed DSM for slender hybrid T-section under pure compression.

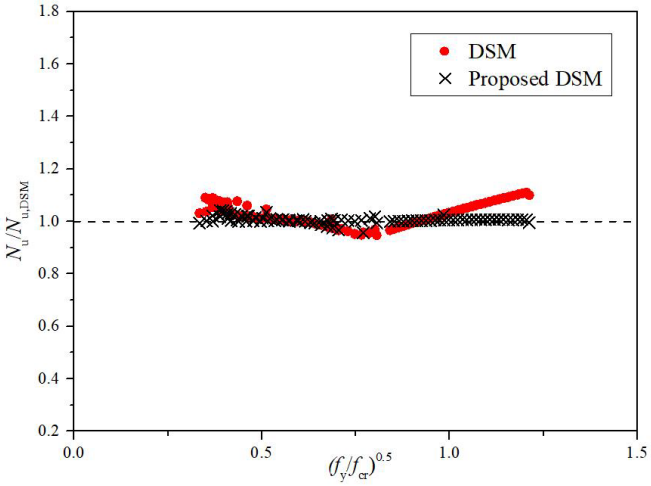

Fig. 25. Comparisons of strength predictions using the DSM and the proposed DSM.

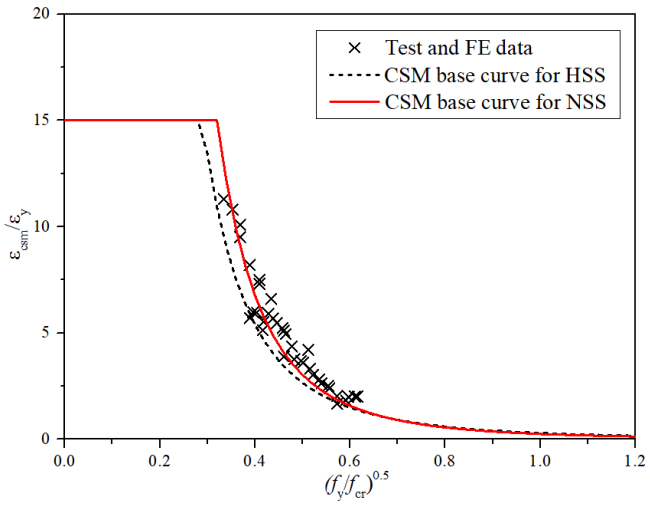

Fig. 26. Assessment of the CSM base curve for for non-slender hybrid T-section under pure compression.

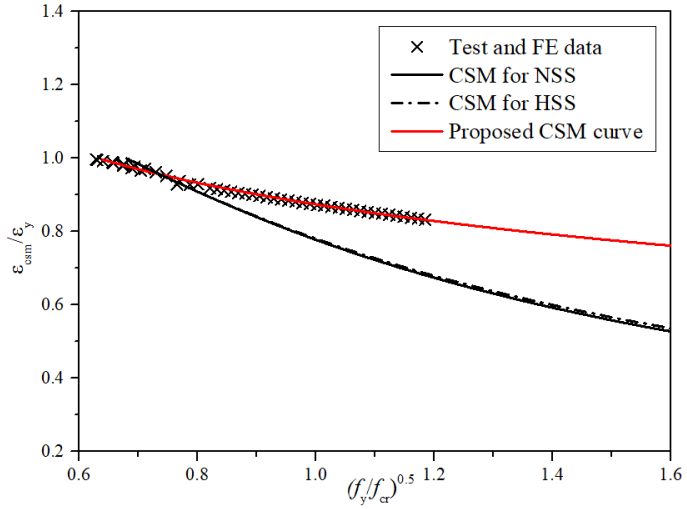

Fig. 27. Assessment of the proposed CSM for slender hybrid T-section under pure compression.

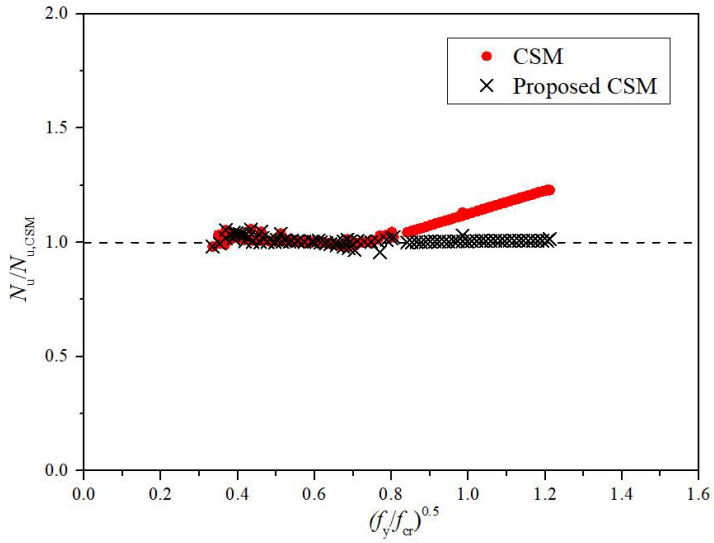

Fig. 28. Comparisons of strength predictions using the CSM and the proposed CSM

5. Reliability analysis

The reliability analysis was carried out in accordance with Annex D of EN 1990 [43] using the first order reliability method (FORM). The CoV of geometric properties was taken as 0.05 in [44]. The key statistical parameters need for conducting the reliability analysis regarding the design codes and design methods are summarised in Table 13. In Table 13, $k_{d,n}$ indicates the design (ultimate limit state) fractile factor, b indicates the mean value of the correction factor, V_δ, indicates the coefficient of variation of the tests and FE simulations relative to the resistance model, V_r is the combined coefficient of variation incorporating both model and basic variable uncertainties and γ_{M0} is the required partial factor. Based on the statistical results in Table 13, it was concluded that CSM requires higher partial factor than DSM. Design approach of DSM provides more accurate predictions than the design codes except for AISC 360-16, despite the higher required partial factor, which are greater than the specified 1.0 in EN 1993-1-1 [19]. The cross-section resistance design based on higher strength steel of flange yield unreliable predictions, particularly for design approach of CSM, which needs partial factor to be 1.21. The proposed modified design approach of DSM and CSM generate reliable predictions with determined partial factor equal to the unity.

Table 13 Comparisons of test and FE results with predicted strengths.

Number of Specimen		N_u /$N_{u,EC3}$	N_u /$N_{u,AISC}$	N_u /$N_{u,AS4100}$	N_u /$N_{u,DSM}$	N_u /$N_{u,DSM}^*$	N_u /$N_{u,CSM}$	N_u /$N_{u,CSM}^*$	N_u /$N_{u,DSM,prop}$	N_u /$N_{u,CSM,prop}$
Test:15	FE:83									
	Mean	1.04	1.01	1.05	1.02	1.16	1.06	1.26	1.01	1.00
	CoV	0.014	0.023	0.019	0.040	0.113	0.069	0.160	0.013	0.013
	$k_{d,n}$	3.194	3.194	3.194	3.194	3.194	3.194	3.194	3.194	3.194
	b	1.04	1.05	1.01	1.02	1.14	1.05	1.21	1.01	1.01
	V_δ	0.014	0.020	0.023	0.040	0.112	0.070	0.158	0.029	0.012
	V_r	0.053	0.055	0.056	0.065	0.123	0.086	0.166	0.059	0.052
	γ_{M0}	0.93	0.96	1.01	1.02	1.05	1.12	1.21	1.00	1.00

6. Conclusions

Experimental and numerical investigations into the local buckling behaviour and cross-section resistances of hybrid T-section stub columns are reported in this paper. The design codes as well as the design approaches were assessed and evaluated. The presented studies allow the following conclusions to be made:

(a) It was found that the codified slenderness limits for outstand flat elements specified in EN 1993-1-1, ANSI/AISC 360-16 and AS 4100 are generally applicable and can be extended for hybrid T-section comprising Q690 flange and Q355 web under pure compression.

(b) All design codes provide consistent but conservative cross-section resistance predictions. AS 4100 provides relatively conservative predictions than the other two design codes. AISC 360-16 yields more accurate predictions with the normalised load ratio close to the unity and become slightly unsafe side when the slenderness is increasing.

(c) The yield slenderness limit based on web strength for design approach of DSM show non-conservative cross-section classification. The yield slenderness limit provided from CSM is closer to limit where the structural performance data converge to the unity. Suitable cross-section yield limit value for DSM and CSM is proposed with $\lambda_p = 0.64$.

(d) CSM provide more accurate results compared with DSM, due to the consideration of strain hardening for non-slender sections. However, over-conservative results are provided when λ_p is greater than 0.68 and the degree of the conservatism is increasing as the slenderness increases.

(e) For cross-section resistance predictions from DSM and CSM, section slenderness λ_p determined using the web strength provide more accurate results than the one derived based on flange strength.

(f) Modifications on the design approaches of DSM and CSM are proposed. The modified DSM and CSM were compared and assessed with the experimental and numerical data. Notable improvements and enhanced reliability have been demonstrated in a reliable manner.

Acknowledgement

The authors would like to thank the help provided from technical staff, Mr. H.Y. Leung from the mechanical workshop and the support from Mr. Li Shuai and Mr. Guo Jiachen.

References

[1] Chen S, Fang H, Liu J-Z, Chan T-M. Design for local buckling behaviour of welded high strength steel I-sections under bending. Thin-Walled Struct. 2022;172:108792.

[2] Liu J-z, Fang H, Chan TM. Experimental investigation on material properties and residual stresses in cold-formed high strength steel irregular octagonal hollow sections. J Constr Steel Res. 2022;191:107170.

[3] Sun Y, Liang Y, Zhao O. Testing, numerical modelling and design of S690 high strength steel welded I-section stub columns. J Constr Steel Res. 2019;159:521-33.

[4] Haaijer G. Economy of high strength steel structural members. J Struct Div. 1961;87:1-24.

[5] Veljkovic M, Johansson B. Design of hybrid steel girders. J Constr Steel Res. 2004;60:535-47.

[6] Ito M, Nozaka K, Shirosaki T, Yamasaki K. Experimental study on moment–plastic rotation capacity of hybrid beams. J Bridge Eng. 2005;10:490-6.

[7] Bartsch H, Eyben F, Pauli G, Schaffrath S, Feldmann M. Experimental and Numerical Investigations on the Rotation Capacity of High-Strength Steel Beams. J Struct Eng. 2021;147:04021067.

[8] Nagarajarao N, Marek P, Tall L. Welded hybrid steel columns. Welding Journal. 1972;51:4625-725.

[9] Naito CJ, Hendricks R, Sause R, Cercone C. Composite steel tee concrete deck bridge system: Design, fabrication, and full-scale verification. J Bridge Eng. 2020;26:04020109.
[10] Li L, Fafard M, Boissonnade N. Local and global instabilities of rolled T-section columns under axial compression. Thin-Walled Struct. 2022;178:109517.
[11] Chen SF. The stem local buckling of T-section compression members. Steel Construction. 2001; 16; 52. (in Chinese)
[12] Chen SF. Interactive local buckling and limiting slenderness of T-strut stem. J Constr Steel Res. 2007; 64: 833-837.
[13]Trahair NS. Post-buckling strength of steel tee columns. Eng Struc. 2013;56:1800-7.
[14] Cao X, Gu L, Kong Z, Zhao G, Wang M, Kim S-E et al. Local buckling of 800 MPa high strength steel welded T-section columns under axial compression. Eng Struc. 2019;194:196-206.
[15] Liu J-z, Chen S, Chan T-M. Testing, numerical modelling and design of Q690 high strength steel welded T-section stub columns. Eng Struc. 2022;259:114142.
[16] Liu J-z, Chen S, Chan T-M. Experimental and numerical investigations of hybrid high strength steel welded T-section stub columns with Q690 flange and Q460 web. Thin-Walled Struct. 2022; 177: 109403.
[17] Yuan L, Zhang Q. Buckling behavior and design of concentrically loaded T-section aluminum alloy columns. Eng. Struc. 2022;260:114221.
[18] EN 1993-1-12, Eurocode 3: Design of Steel Structures – Part 1–12: Additional Rules for the Extension of EN 1993 up to Steel Grades S700. Brussels: European Committee for Standardization (CEN); 2007.
[19] EN 1993-1-1, Eurocode 3: Design of Steel STRUCTURES – Part 1.1: General Rules and Rules for Buildings. Brussels: European Committee for Standardization (CEN); 2005.
[20] EN 1993-1-5, Eurocode 3: Design of Steel Structures – Part 1–5: Plated structural elements. Brussels: European Committee for Standardization (CEN); 2006.
[21] EN ISO 6892-1, Metallic Materials – Tensile Testing Part 1: Method of Test at Ambient Temperature. EN ISO 6892-1. Brussels, Belgium: CEN; 2019.
[22] Liu J-z, Fang H, Chen S, Chan T-M. Material properties and residual stresses of high strength steel hexagonal hollow sections. J Constr Steel Res. 2022;190:107061.
[23] Liu J-z, Fang H, Chan TM. Investigations on material properties and residual stresses in cold-formed high strength steel irregular hexagonal hollow sections. Thin-Walled Struct. 2022;176: 109220.
[24] Chen J, Zhu J-Y, Chan T-M. Experimental and numerical investigation on stub column behaviour of cold-formed octagonal hollow sections. Eng Struc. 2020;214:110669.
[25] Liu J-z, Fang H, Chan TM. Experimental investigations on material properties and stub column behaviour of high strength steel irregular hexagonal hollow sections. J Constr Steel Res. 2022;196: 107343.
[26] Ziemian RD. Guide to stability design criteria for metal structures: John Wiley & Sons; 2010.
[27] Totten GE. Handbook of residual stress and deformation of steel. ASM International 2002.
[28] Chan TM, Gardner L. Compressive resistance of hot-rolled elliptical hollow sections. Eng Struc. 2008;30:522-32.
[29] Gardner L, Nethercot DA. Experiments on stainless steel hollow sections—Part 1: Material and cross-sectional behaviour. J Constr Steel Res. 2004;60:1291-318.
[30] Ma JL, Chan TM, Young B. Design of Cold-Formed High-Strength Steel Tubular Stub Columns. J Struct Eng. 2018;144(6): 04018063.
[31] Fang H, Chan T-M. Buckling resistance of welded high-strength-steel box-section members under combined compression and bending. J Constr Steel Res. 2019;162: 105711.
[32] Liu J-z, Fang H, Chan TM. Structural behaviour of high strength steel hexagonal hollow section stub columns under axial compression. Eng Struc. 2022; 268: 114653.
[33] Liu J-z, Fang H, Chan TM. Experimental and numerical investigations on stub column behaviour of cold-formed high strength steel irregular octagonal hollow sections. Thin-Walled Struct. 2022; 180: 109770.
[34] ANSI/AISC 360-16, Specification for Structural Steel Buildings. Chicago: American Institute of Steel Construction (AISC); 2016.
[35] AS 4100-1998(R2016), Steel structures (Reconfirmed 2016 Incorporating Amendment No.1), AS 4100. Sydney,

817 Australia: Australian Standard; 2016.
818 [36]Schafer B, Peköz T. Computational modeling of cold-formed steel: characterizing geometric imperfections and
819 residual stresses. J Constr Steel Res. 1998;47:193-210.
820 [37] Gardner L, Ashraf M. Structural design for non-linear metallic materials. Eng Struc. 2006;28:926-34.
821 [38] Buchanan C, Gardner L, Liew A. The continuous strength method for the design of circular hollow sections. J
822 Constr Steel Res. 2016;118:207-16.
823 [39] Zhao O, Gardner L, Young B. Behaviour and design of stainless steel SHS and RHS beam-columns. Thin-Walled
824 Struct. 2016;106:330-45.
825 [40] Lan X, Chen J, Chan T-M, Young B. The continuous strength method for the design of high strength steel tubular
826 sections in compression. Eng Struc. 2018;162:177-87.
827 [41] Yun X, Gardner L, Boissonnade N. The continuous strength method for the design of hot-rolled steel crosssections.
828 Eng Struc. 2018;157:179-91.
829 [42] Yun X, Gardner L. Stress-strain curves for hot-rolled steels. J Constr Steel Res. 2017;133:36-46.
830 [43] EN 1990. Eurocode - Basis of structural design. Brussels, Belgium: European Committee for Standardization (CEN);
831 2002.
832 [44] Afshan S, Francis P, Baddoo NR, Gardner L. Reliability analysis of structural stainless steel design provisions. J
833 Constr Steel Res. 2015;114:293-304.